THE ASTROPHYSICAL JOURNAL, 460:408–436, 1996 March 20

CORE-COLLAPSE SUPERNOVAE AND THEIR EJECTA

FRIEDRICH-KARL THIELEMANN
Institut für theoretische Physik, Universität Basel, Klingelbergstrasse 82, CH-4056 Basel, Switzerland;
fkt@quasar.physik.unibas.ch

KEN'ICHI NOMOTO
Department of Astronomy and Research Center for the Early Universe School of Science, University of Tokyo, Bunkyo-ku, Tokyo 113, Japan; nomoto@astron1.astron.s.u-tokyo.ac.jp

AND

MASA-AKI HASHIMOTO
Department of Physics, Faculty of Science, Kyushu University, Fukuoka 810, Japan;
e76051a@kyu-cc.cc.kyushu-u.ac.jp

Received 1994 August 18; accepted 1995 September 18

ABSTRACT

We present the detailed isotopic composition for 13, 15, 20, and 25 $M_\odot$ stars, based on induced supernova calculations, which lead to explosive Si, O, Ne, and C burning during the supernova outburst. The calculations made use of inferred mass cuts between the central neutron star and the ejected envelope by requiring ejected ^{56}Ni masses in agreement with supernova light curve observations. Specific emphasis is put on the treatment of the innermost layers, which experience complete Si burning with an alpha-rich freezeout and are the source of ^{56}Ni, the Fe group composition in general, and some intermediate-mass alpha elements like Ti. However, the uncertainty of the mass cut and the delay time between core collapse and the explosion via neutrino heating put limits on the possible accuracy. The predictions are compared with abundances from specific supernova observations (e.g., SN 1987A, 1993J) or supernova remnants (e.g., G292.0+1.8, N132D). The amount of detected ^{16}O and ^{12}C or products from carbon and explosive oxygen burning can constrain our knowledge of the *effective* ^{12}C(α, γ)^{16}O rate in He burning. The ^{57}Ni/^{56}Ni ratio (observed via γ-rays from ^{56,57}Co decay or spectral features changing during the decay) can give constraints on Y_e in the innermost ejected zones. This helps to locate the position of the mass cut and to estimate the necessary delay time between collapse and explosion, in order to permit the required mass accretion $\Delta M_{\rm acc}$. Provided that the stellar precollapse models are reliable, this allows additional insight into the exact working of the supernova explosion mechanism. While this has been only possible for one supernova until present (SN 1987A, a 20 $M_\odot$ star), we can also compare the ejected composition from other progenitor masses to abundances in low-metallicity stars, which reflect the average Type II supernova composition, integrated over an initial mass function of progenitor stars.

Subject headings: nuclear reactions, nucleosynthesis, abundances — stars: interiors — stars: neutron — supernovae: general

1. INTRODUCTION

Except for Type Ia supernovae, which are explained by exploding white dwarfs in binary systems, all other supernova types (Ib/IIb, Ic, II-L, and II-P) seem to be linked to massive stars with main-sequence masses $M > 8\ M_\odot$ (e.g., Hashimoto, Iwamoto, & Nomoto 1993a). All stars in that mass range produce a collapsing Fe core after the end of their hydrostatic evolution, which proceeds to nuclear densities. The Fe core results either from hydrostatic Si burning or Ne, O, and Si burning in the collapse of a degenerate ONeMg core, triggered by electron captures on ^{20}Ne and ^{24}Mg. In most cases, a central neutron star (or black hole) will result and the envelope is ejected when a shock wave forms, most probably powered by neutrinos which release the gravitational binding energy of the (proto)neutron star. This paper concentrates on the composition of the ejecta from such core-collapse supernovae and is an extension of calculations for a 20 $M_\odot$ star (Hashimoto, Nomoto, & Shigeyama 1989; Thielemann, Hashimoto, & Nomoto 1990) and preliminary estimates for an appreciably larger range of progenitor masses (Thielemann, Nomoto, & Hashimoto 1993, 1994b; Hashimoto et al. 1993b).

One of the still uncertain parameters in stellar evolution, and thus for the presupernova models, is the ^{12}C(α, γ)^{16}O reaction (see Filippone, Humblet, & Laganke 1989; Caughlan et al. 1985; Caughlan & Fowler 1988; Barker & Kajino 1991; Buchmann et al. 1993; Zhao et al. 1993a, b; Azuma et al. 1994; Mohr et al. 1995). The combined effects of this reaction and the treatment of overshooting and semiconvection, which governs the growth of the helium-burning core, determine the composition and the structure of the precollapse star. The mixing of fresh He fuel into the He-burning core at late stages and high temperatures, when a core without growth by semiconvection and overshooting of convective eddies would have already ceased to possess any He fuel, probes the ^{12}C(α, γ)^{16}O rate at higher temperatures and turns much of the remaining ^{12}C into ^{16}O (see, e.g., d'Antona & Mazzitelli 1991; Langer & Henkel 1994). Thus, the amount of ^{12}C and ^{16}O produced by a star depends on the nuclear rate *and* the treatment of convection in a combined way, which hopefully can be disentangled in the future. The calculations presented here are based on stellar models which employed the rate of Caughlan et al. (1985), the Schwarzschild criterion of convection, and no overshooting, described in detail in Nomoto & Hashimoto (1988) and Hashimoto et al. (1993b). We will discuss this

choice together with the nucleosynthesis results and show that it predicts results in very good agreement with observations.

The most desirable way to perform explosive nucleosynthesis calculations in SNe II would include a hydrodynamic calculation, following the Fe core collapse, the bounce at nuclear densities, the propagating shock wave until it turns into an accretion shock, the leakage of neutrinos from the proto–neutron star, neutrino heating, and a delayed explosion with a shock passing through the envelope to be ejected. However, until recently there existed still a number of open problems with the supernova mechanism of massive stars (see, e.g., Bruenn 1989a, b; Cooperstein & Baron 1989; Baron & Cooperstein 1990; Myra 1988; Myra & Bludman 1989; Wilson & Mayle 1988, 1993; Mayle & Wilson 1988, 1990; Bethe 1990; Bruenn & Haxton 1991). Only very recently could independent groups (Janka 1993) reproduce this delayed shock scenario, although the explosion energies in spherically symmetric explosion calculations were still on the low side. The convective turnover seen, e.g., by Herant et al. (1994), Janka & Müller (1995), and Burrows, Hayes, & Fryxell (1995) in multidimensional calculations can enhance the neutrino luminosity and guarantee an explosion (Burrows & Goshy 1993) and might also lead to the correct explosion energies and finally solve the SNe II puzzle. An essential parameter describing the delayed explosion mechanism is the delay time t_{de} between the core bounce at nuclear densities and the explosion via neutrino heating, which depends on the details of neutrino transport. The delay time t_{de} is highly important for the composition of the ejecta, and its behavior as a function of stellar mass is still an open question, especially as two-dimensional calculations might not yet be "converged."

While the progress and qualitative improvement seem obvious, the quantitative results with respect to the exact value of the delay time t_{de} might still have uncertainties, dependent in general on (i) the equation of state, which can affect the convective stability of mass zones, (ii) the numerical resolution and/or treatment of neutrino transport in multidimensional calculations, or (iii) the possibly not justified application of mixing-length theory in spherically symmetric calculations. Therefore, we still want to make use of the fact that typical energies of 10^{51} ergs are observed and light-curve as well as explosive nucleosynthesis calculations can be performed with an artificially induced shock wave of appropriate energy, applied to the precollapse stellar model (see, e.g., Woosley & Weaver 1986, 1994; Shigeyama, Nomoto, & Hashimoto 1988; Woosley 1988; Woosley, Pinto, & Weaver 1988; Hashimoto et al. 1989; Arnett & Fu 1989; Thielemann et al. 1990; Hashimoto et al. 1993b; Weaver & Woosley 1993; Thielemann et al. 1994b). There will, of course, be a variation of this value with progenitor mass, but only by a small factor. The temperatures at a given radius, obtained during the propagation of a shock front, are proportional to $E^{1/4}$ (see § 2). Thus, we expect that this uncertainty introduces small errors. Larger uncertainties are expected from the missing knowledge of the exact core structure at the time at which the shock wave starts propagating outward. The lack of knowledge of the shock initiation introduces an additional uncertainty, because different ways of initiating the explosion (piston, thermal, or kinetic energy deposition) can lead to different results. Aufderheide, Baron, & Thielemann (1991) have studied these questions in detail and came to the conclusion that errors in the bulk composition of up to 30% are introduced. While this is not negligible, it is small enough in order to proceed with nucleosynthesis studies before a full understanding of the SNe II mechanism.

One remaining problem when performing calculations with initiated shock waves cannot be avoided. The location of the mass cut between neutron star and ejected envelope is uncertain. It can be determined from observational constraints, which give clues to the ejected mass of ^{56}Ni, but it depends also on the delay time between bounce and delayed explosion, because during this period the proto–neutron star grows by accretion. In this paper we make use of the guidance by observational contraints for individual supernovae as a function of progenitor mass. Other approaches are possible (see Timmes, Woosley, & Weaver 1995). They all have to pass a crucial test, given by the abundances of low metallicity stars in our Galaxy, which are essentially determined by SNe II nucleosynthesis (see § 4, especially § 4.3).

In case of SN 1987A (20 $M_\odot$ during the main-sequence stage), the light curve, powered by decaying ^{56}Ni and ^{56}Co, could be utilized to determine the mass of ^{56}Ni produced (0.075 ± 0.01 $M_\odot$; see, e.g., Arnett et al. 1989), which is located in the innermost zones of the ejecta and therefore provides information about the mass cut. SN 1993J (a 14 ± 1 $M_\odot$ star during main sequence) is another case, in which the ^{56}Ni mass is reasonably well established (0.1 ± 0.02 $M_\odot$; Baron, Hauschildt, & Young 1995; Nomoto, Iwamoto, & Suzuki 1995). For progenitors of different mass, where such information is not available, we have to search for other sources of information. Type Ib and Ic supernova light curves, which owing to the lack of a large H envelope and their early X-ray and gamma-ray losses are steeper than those of SNe II, can give an estimate of the He core mass. Typical SNe Ib/Ic, indicating a main-sequence progenitor mass of about 12–16 $M_\odot$, seem to require the ejection of ≈ 0.15 $M_\odot$ of ^{56}Ni (see, e.g., Panagia 1987; Shigeyama et al. 1990; Nomoto, Filippenko, & Shigeyama 1990; Nomoto et al. 1994). An additional tendency, although not a direct quantitative information, of a decreasing mass of ^{56}Ni ejecta with decreasing expansion velocities, i.e., increasing progenitor masses (Schmidt 1995), can be used as guidance to extrapolate the mass of the Ni ejecta for more massive SNe II.

We ignore with our approach the very small but important amount of matter in the high-entropy bubble, where neutrino heating and neutronization can cause conditions which lead to the production of *r*-process nuclei (Woosley & Hoffman 1992; Meyer et al. 1992; Kratz et al. 1993; Thielemann et al. 1994a; Witti, Janka, & Takahashi 1994; Takahashi, Witti, & Janka 1994; Woosley et al. 1994; Chen et al. 1995). These very innermost mass zones of the high-entropy bubble quite possibly require a multidimensional treatment. At present we leave these questions aside and follow the more conventional treatment discussed above. This is possible because the high-entropy bubble contains negligible amounts of matter ($< 10^{-3}$ $M_\odot$), mostly important for *r*-process nuclei, and the shock forms beyond the high-entropy bubble in a spherical manner (Herant et al. 1994).

In an earlier paper (Thielemann et al. 1994b), we gave preliminary results for 13, 15, 20, and 25 $M_\odot$ stars with a detailed isotopic composition only for matter which experienced incomplete Si burning but regular O, Ne, and C

burning during the supernova outburst. This alone underestimates nuclei like ^{44}Ti (^{44}Ca after decay), ^{48}Cr (^{48}Ti), and ^{52}Fe (^{52}Cr) and cannot give the detailed composition of Fe group nuclei. Here we attempt to address this issue and give the best possible answer for the innermost layers of complete Si burning with alpha-rich freezeout, which are important for the production of ^{56}Ni, the Fe group composition in general, including the intermediate-mass alpha elements discussed above, as far as the uncertainty of the mass cut between the neutron star and the ejecta allows it.

Taking into account all the constraints discussed above, we can present the composition of SNe II over an appreciable range of progenitor masses. We compare the results from individual models with abundances observations for specific supernovae (i.e., SN 1987A, 1993J) or supernova remnants (e.g., G292.0+1.8, N132D), where the amount of detected ^{16}O and ^{12}C or products from carbon and explosive oxygen burning can constrain our knowledge of the *effective* ^{12}C(α, γ)^{16}O rate in He burning. The ^{57}Ni/^{56}Ni ratio (observed via γ-rays from ^{56,57}Co decay or spectral features changing during the decay time) can give constraints on Y_e in the innermost ejected zones and with it the position of the mass cut and the necessary delay time between collapse and explosion driven by neutrino heating. This allows additional insight into the exact working of the supernova explosion mechanism.

Finally, we can compare the ejected composition to abundances in low-metallicity stars. They reflect the average SNe II composition and are a constraint which has to be met by any theory, after integrating the ejecta composition over an initial mass function of progenitor stars. The present paper, however, does not yet present a dense and extended enough set for such a quantitative comparison. This will be contained in a forthcoming paper (Hashimoto et al. 1995), in which the overall agreement will also be discussed as a function of the nuclear ^{12}C(α, γ) rate and variations in the explosion energy, and the influence of different convection treatments will be examined. The present paper focuses on the discussion of individual models and the Fe-group composition and mass-cut constraints.

2. EXPLOSIVE NUCLEOSYNTHESIS AND THE MASS CUT

2.1. *Basic Features and Expected Outcome*

The calculations were performed by depositing a total thermal energy of the order $E = 10^{51}$ ergs plus the gravitational binding energy of the ejected envelope into several mass zones of the stellar Fe core (for details, see Shigeyama et al. 1988). This calculation made use of a hydro code and a very simple network of alpha nuclei to give an accurate nuclear energy generation. In a second step of *postprocessing*, the temperature and density profile of each mass zone was followed with a full network, containing 299 nuclear species as described in Thielemann et al. (1990). That means that this paper only deals with the nucleosynthesis of nuclei with $A < 77$. Electron and positron capture rates by Fuller, Fowler, & Newman (1980, 1982, 1985) for nuclei with mass numbers between $A = 20$ and $A = 60$ have been used. Experimental nuclear rates for light nuclei came from the most recent rate compilation by Caughlan & Fowler (1988), experimental neutron capture cross sections come from Bao & Käppeler (1987) and Beer, Voss, & Winters (1992). Rate tables for unstable light nuclei from Malaney & Fowler (1988, 1989), Wiescher et al. (1986, 1987, 1989, 1990), Rauscher et al. (1994), and van Wormer et al. (1994) were included. For the vast number of medium and heavy nuclei which exhibit a high density of excited states at capture energies, statistical model (Hauser-Feshbach) calculations are applicable. The most recent compilation by Thielemann, Arnould, & Truran (1987) was employed (for a detailed discussion of the input physics see Cowan, Thielemann, & Truran 1991).

As discussed above, the most significant parameter in explosive nucleosynthesis is the temperature, and a good qualitative understanding of the composition can already be gained by knowing only T_{max}, without having to perform complex nucleosynthesis calculations. Weaver & Woosley (1980) already recognized that matter behind the shock front is strongly radiation dominated. Assuming an almost homogeneous density and temperature distribution behind the shock (which is approximately correct; see Fig. 3 in Shigeyama et al. 1988), one can equate the supernova energy with the radiation energy inside the radius r of the shock front

$$E_{SN} = \frac{4\pi}{3} r^3 a T(r)^4 . \quad (1)$$

This equation can be solved for r. With $T = 5 \times 10^9$ K, the lower bound for explosive Si burning with complete Si exhaustion, and $E_{SN} = 10^{51}$ ergs, the result is $r \approx 3700$ km (see Woosley 1988). For the evolutionary model by Nomoto & Hashimoto (1988) of a 20 $M_\odot$ star, this radius corresponds to 1.7 $M_\odot$, in excellent agreement with the exact hydrodynamic calculation (see Thielemann et al. 1990). Temperatures which characterize the edge of the other explosive burning zones correspond to the following radii: incomplete Si burning ($T_9 = 4$, $r = 4980$ km), explosive O burning (3.3, 6430), and explosive Ne/C burning (2.1, 11,750). This relates to masses of 1.75, 1.81, and 2.05 $M_\odot$ in the case of the 20 $M_\odot$ star. The radii mentioned are model independent and vary only with the supernova energy.

When applying the same procedure to other SN II progenitor models by Nomoto & Hashimoto (1988), and assuming an average supernova energy of 10^{51} ergs, the masses in Table 1 result. Table 1 can be understood in the following way. Matter between the mass cut $M(r) = M_{cut}$ and the mass enclosed in the radius corresponding to explosive Si burning with complete Si exhaustion is indicated with M(ex Si-c). Then follows the zone of incomplete Si

TABLE 1

MASSES IN EXPLOSIVE AND HYDROSTATIC BURNING

	BURNING SITE	13M$_\odot$	15M$_\odot$	20M$_\odot$	25M$_\odot$
M(Fe-core)	hydrostatic Si-burning	1.18	1.28	1.40	1.61
M_{cut}		?	?	1.61	?
M(ex Si-c)	explosive Si-burning	1.42	1.46	1.70	1.79
M(ex Si-i)	incomplete Si-burning	1.48	1.52	1.75	1.85
M(ex O)	explosive O-burning	1.54	1.57	1.81	1.92
M(ex Ne)	explosive Ne/C-burning	1.66	1.73	2.05	2.26
M(C-core)	hydrostatic He-burning	1.75	2.02	3.70	5.75
	MAIN PRODUCTS				
ΔM(ex Si-c)	"Fe", He	?	?	0.09	?
ΔM(ex Si-i)	Si, S, Fe, Ar, Ca	0.06	0.06	0.05	0.06
ΔM(ex O)	O, Si, S, Ar, Ca	0.06	0.05	0.06	0.07
ΔM(ex Ne)	O, Mg, Si, Ne	0.12	0.16	0.24	0.34
ΔM(C-core)	O, Ne, Mg, Si	0.09	0.29	1.65	3.49

burning until M(ex Si-i), explosive O burning until M(ex O), explosive Ne/C burning until M(ex Ne), and unprocessed matter from the C/Ne core is ejected until M(C-core). In all cases, the total masses enclosed in a radius r are listed (in units of $M_\odot$). The masses ΔM between these burning radii, which are involved in the different explosive burning phases, are displayed in the second part of Table 1, where the most abundant elements in these zones are also listed. As discussed before, we do not know a priori where the mass cut is located, and therefore we cannot predict the total amount of ejected matter which experienced complete Si burning (Si-c). The values listed for a 20 $M_\odot$ star have been chosen to reproduce the 0.07 $M_\odot$ of ^{56}Ni deduced from light-curve observations of SN 1987A (see, e.g., Arnett et al. 1989; McCray 1993). The choice for the other progenitor masses will be discussed below, but their uncertain nature is underlined with a question mark. The zones beyond explosive Ne/C burning ($T_{max} < 2.1 \times 10^9$ K) are essentially unaltered, and the composition is almost identical to the preexplosive one. It is clearly recognizable that the amount of ejected mass from the unaltered (essentially only hydrostatically processed) C core varies strongly over the progenitor mass range. The variation is still large for the matter from explosive Ne/C burning, while the amount of mass from explosive O and Si burning is almost the same for all massive stars.

The average composition for major elements in individual explosive burning stages, based on the calculations for a 20 $M_\odot$ star (Thielemann et al. 1990) is displayed in Table 2. They represent typical mass fractions which should be expected in explosive Si and O burning zones. For the zones containing only hydrostatically processed material, we expect a changing C to O ratio, reflecting the increasing temperatures in core He burning of more massive stars and with it a different efficiency of the $^{12}C(\alpha, \gamma)^{16}O$ rate. Ne and Mg as products of C burning could change as well, and thus the C, O, Ne, and Mg abundances are not necessarily represented correctly by those of a 20 $M_\odot$ star.

Apart from these exceptions, one can get a rough idea about abundance yields for a wide mass range of SN II progenitors, when taking the masses ΔM from Table 1 for the individual burning zones and multiplying them with the mass fractions given in Table 2. The explosive yields should be quite insensitive to this procedure and quite accurate because they depend mostly on the peak temperatures and densities. The neutron excess of matter, $\eta = \sum_i (N_i - Z_i) Y_i$ or the electron fraction $Y_e = \sum_i Z_i Y_i$, Y_i denoting the abundance of the nucleus (Z_i, A_i), which is also influencing the resulting composition, is very similar outside the O-burning shell for different stellar masses. The matter which undergoes complete Si burning is located close to a transition in the neutron excess from electron captures in the O-burning shell. The mass cut between the finally remaining neutron star and the ejecta, determining the neutron excess in explosive burning and the composition of the Fe group, depends on the details of the explosion mechanism. The choice of Fe(Ni) ejecta is discussed in § 2.2, and the values indicated by an asterisk are only estimates. This can change the fraction of Fe produced in complete Si burning and will be discussed in §§ 3 and 4.

A first overview of the actual results from the explosion calculations (given in more detail in § 3) is displayed in Table 3 for elemental abundances. They reflect exactly the behavior discussed above in Tables 1 and 2: the amount of ejected mass from the unaltered (essentially only hydrostatically processed) C core and from explosive Ne/C burning (C, O, Ne, Mg) varies strongly over the progenitor mass range, while the amount of mass from explosive O and Si burning (S, Ar, and Ca) is almost the same for all massive stars. Si has some contribution from hydrostatic burning and varies by a factor of 2–3. The amount of Fe-group nuclei ejected depends directly on the explosion mechanism. Thus, we have essentially three types of elements, which test different aspects of supernovae when comparing with individual observations. The first set (C, O, Ne, Mg) tests the stellar progenitor models, the second (Si, S, Ar, Ca) tests the progenitor models and the explosion energy in the shock wave, while the Fe group (beyond Ti) also probes clearly the actual supernova mechanism. Only when all three aspects of the predicted abundance yields can be verified with individual observational checks will it be reasonably secure to utilize these results in chemical evolution calculations of galaxies.

In general, we should keep in mind that as long as the explosion mechanism is not completely and quantitatively understood yet, one has to assume a position of the mass cut, and dependent on that position which is a function of the delay time between collapse and final explosion, the ejected mass zones will have a different neutron excess. We will discuss this in more detail in the following subsections.

2.2. *Inferred Mass Cuts*

Type II supernova explosions, the endpoint of the evolution of massive stars, lead to the formation of neutron stars or black holes (for a review, see, e.g., Bethe 1990) depending on the size of the collapsing Fe core, the delay time between collapse and explosion, and the permitted maximum neutron star mass, which is somewhat uncertain and related to the still-limited understanding of the nuclear equation of state beyond nuclear densities (e.g., Glendenning 1991; Weber & Glendenning 1991; Brown & Bethe 1994). Appar-

TABLE 2

TYPICAL MASS FRACTIONS OF ELEMENTS IN BURNING SITES

Element	C-core	ex Ne	ex O	ex Si-i	ex Si-c
O	0.72	0.80	0.45		
Ne	0.13	0.04			
Mg	0.09	0.08	0.005		
Si	0.02	0.08	0.30	0.40	
S			0.20	0.25	
Ar			0.025	0.06	
Ca			0.02	0.05	
Fe				0.20	0.70

TABLE 3

MAJOR NUCLEOSYNTHESIS YIELDS

Element	13$M_\odot$	15$M_\odot$	20$M_\odot$	25$M_\odot$
C	0.060	0.083	0.115	0.148
O	0.218	0.433	1.480	3.000
Ne	0.028	0.039	0.257	0.631
Mg	0.012	0.046	0.182	0.219
Si	0.047	0.071	0.095	0.116
S	0.026	0.023	0.025	0.040
Ar	0.0055	0.0040	0.0045	0.0072
Ca	0.0053	0.0033	0.0037	0.0062
Fe	*0.150*	*0.130*	0.075	*0.050*

ently, collapse calculations with the best available microphysics do not lead to successful explosions with the prompt mechanism, in which the shock wave, created at the edge of the collapsed core at bounce, can cause the ejection of the outer envelope (see, e.g., Cooperstein and Baron 1989; Bruenn & Haxton 1991). The remaining promising mechanism is the delayed explosion mechanism, caused by neutrino heating on a timescale of seconds or less. The exact delay time depends on the question of whether neutrinos diffuse out from the core (>0.5 s), weak convection occurs as a result of composition gradients ("saltfinger convection"), or convective turnover owing to entropy gradients shortens this escape time substantially (Wilson & Mayle 1988, 1993; Mayle & Wilson 1988, 1990; Herant et al. 1994; Janka & Müller 1995; Burrows et al. 1995). As it has become possible by now to obtain direct information about the mass cut between the forming neutron star and the ejected envelope for a number of specific supernovae for which the progenitors are known, we can start to draw conclusions on the mechanism and the amount of Fe ejecta as a function of progenitor mass.

Three sets of arguments are helpful with respect to neutron star masses:

1. Core Si burning leads typically to values of the electron fraction $Y_e = \sum_i Z_i Y_i = \langle Z/A \rangle$, which produce an abundance composition which cannot be a major component of solar abundance composition which cannot be a major component of solar abundances (see Thielemann & Arnett 1985 or also Trimble 1975). Also, the Fe-group composition of low-metallicity stars (reflecting the early evolution of the Galaxy where only SN II events occurred) does not allow for such matter to be a main component of SN II ejecta (see the discussion in § 4). Only minor amounts, of the order of 10^{-5} to 10^{-6} $M_\odot$ of neutron-rich matter in form of r-process elements or Fe-group nuclei, are allowed to be ejected per SN II event. This is negligible and does not affect any consideration of neutron star masses. Therefore, the absolute lower limit for neutron star masses from SN II explosions is given by the Fe core masses of progenitor stars. This information is available from a grid of stellar models at the onset of Fe core collapse (e.g., Nomoto & Hashimoto 1988; Weaver & Woosley 1993; Hashimoto et al. 1993b; see also Table 1).

2. Explosive nucleosynthesis calculations predict the products of explosive C, Ne, O, and Si burning. Si burning with complete Si exhaustion leads to the dominant formation of ^{56}Ni for $Y_e > 0.49$ (Woosley, Arnett, & Clayton 1973, or § 2.3). This is the ^{56}Ni which powers the light curve of all supernovae with its decay to ^{56}Co and ^{56}Fe. With known distances to supernovae, one can deduce the required amount of ^{56}Ni. In the case of SN 1987A, it was 0.075 ± 0.01 $M_\odot$, and for SN 1993J it is 0.1 ± 0.02 $M_\odot$ (Nomoto et al. 1993; Shigeyama et al. 1994; Woosley et al. 1994; Young, Baron, & Branch 1995) for a distance of 3.6 ± 0.3 Mpc (Freedman et al. 1994) and the correct extinction (Clocchiatti et al. 1995). In both cases, the mass of the progenitor star is also known, being of the order 20 $M_\odot$ and 14 ± 1 $M_\odot$, respectively. As ^{56}Ni is produced in the innermost ejected zones which experience the highest temperatures, an integration of the explosive nucleosynthesis products for a specific stellar model will imply the location of the mass cut between ejected envelope and remaining neutron star (see, e.g., Thielemann et al. 1990).

3. SNe Ib and SNe Ic seem to be events related to the core collapse of massive stars, but without H envelope (Ib) and even without (or only with a minute) He envelope (Ic), therefore being classified as SNe I. The steepness of their light curves, deviating already early from the pure exponential decline with the ^{56}Co half-life, indicates small He cores between 3 and 4 $M_\odot$, which qualify them as originating from about 12–16 $M_\odot$ progenitor stars. Such stars do not lose their H envelope as single stars by a strong stellar wind (Wolf-Rayet star), but only in binary systems (for details see the discussion in Nomoto et al. 1990; Panagia 1987; Shigeyama et al. 1990; Wheeler & Harkness 1990). The light-curve information requires ejected ^{56}Ni masses of ≈ 0.15 $M_\odot$ for both events, when taking the extinction from Jeffery et al. (1991) and $H_0 = 60$ km s^{-1} Mpc^{-1} for SN Ic 1987M and $0.07^{+0.035}_{-0.025}$ $M_\odot$ for SN Ic 1994I, if we take the approach of Iwamoto et al. (1994). These are comparable to the 0.075 $M_\odot$ for SN 1987A, a 20 $M_\odot$ star, and the 0.1 $M_\odot$ for SN 1993J, a 15 $M_\odot$ star. This gives information for some grid points in the mass spectrum of SNe II progenitors. They allow presently an interpretation in terms of Ni ejecta in form of an either slightly declining function of progenitor mass (0.15–0.075 $M_\odot$ over the mass range 13–20 $M_\odot$), or a relatively constant function with values between 0.07 and 0.1 $M_\odot$ in the same mass range. Our choice in Table 3 represents the first option. The available information for intermediate-mass elements like O-Ca, which are not affected by the choice of a mass cut, and the known ratios of [O/Fe] through [Ca/Fe] from abundance observations in low-metallicity stars [Fe/H] ≤ -1, give an additional constraint on the permitted or required Ni(Fe) integrated over all SN II progenitor masses and thus set limits for the Fe ejecta of a 25 $M_\odot$ star and more massive stars. The amount of Fe, deduced from X-ray observations of supernova remnants, can also give additional constraints (see § 4).

2.3. *Explosive Nucleosynthesis and* Ni(Fe) *Ejecta*

Hashimoto et al. (1989) and Thielemann et al. (1990) performed explosive nucleosynthesis calculations for a 20 $M_\odot$ star (6 $M_\odot$ He core) and obtained detailed nucleosynthesis products (for a comparison, see also Woosley et al. 1988). The outer boundary of explosive Si burning with complete Si exhaustion was located at 1.7 $M_\odot$, where temperatures of 5×10^9 K are attained. A pure ^{56}Ni composition inside this boundary would require the mass cut to be at 1.63 $M_\odot$ with the ejection of 0.07 $M_\odot$ of ^{56}Ni. Making use of the slightly more neutron-rich composition within the vicinity of the Si-burning shell (smaller Y_e) can reduce somewhat the mass fraction of ^{56}Ni. In order to obtain the same ^{56}Ni ejection, a slightly deeper mass cut can be required.

Here we want to present additional calculations for 13, 15, and 25 $M_\odot$ stars (3.3, 4, and 8 $M_\odot$ He cores, respectively) and also take into account the possible effect of the delayed explosion mechanism on the Y_e of the innermost ejecta. The results for the whole mass sequence are shown in Figures 1*a*–1*f*. Only the dominant abundances of intermediate-mass nuclei are plotted. We refer to the detailed plots (Figs. 7–8) in Thielemann et al. (1990) for a more extensive account of isotopic abundances resulting from Ne/C and O burning. In this paper we focus on the Fe-group abundances and their behavior as a function of Y_e, depending again on the explosion mechanism and delay time between collapse and explosion via neutrino heating.

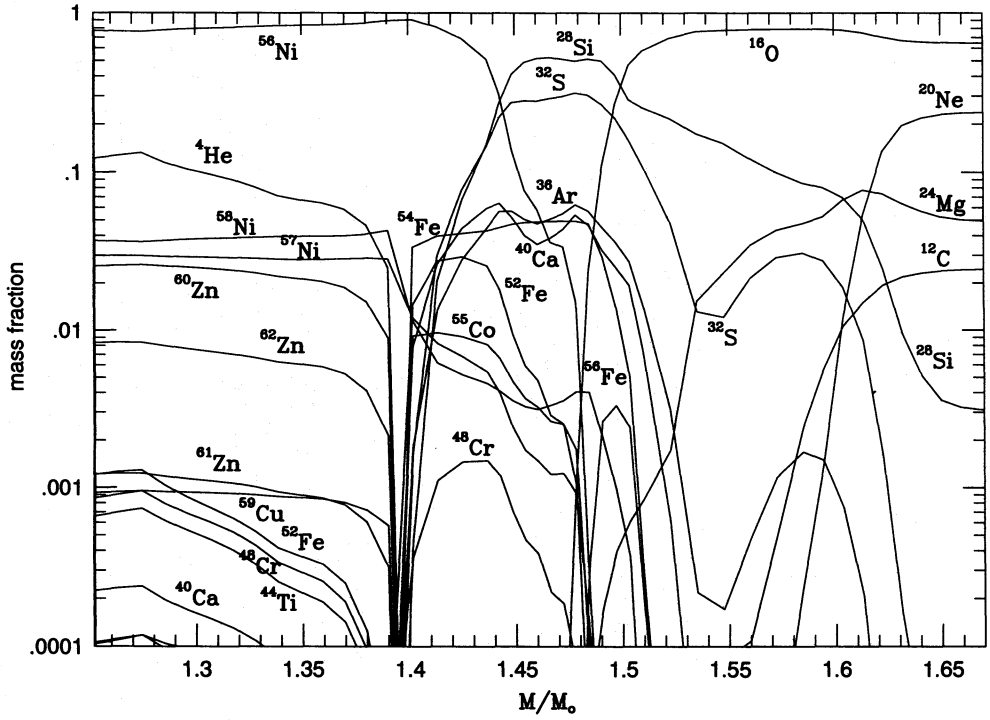

FIG. 1*a*

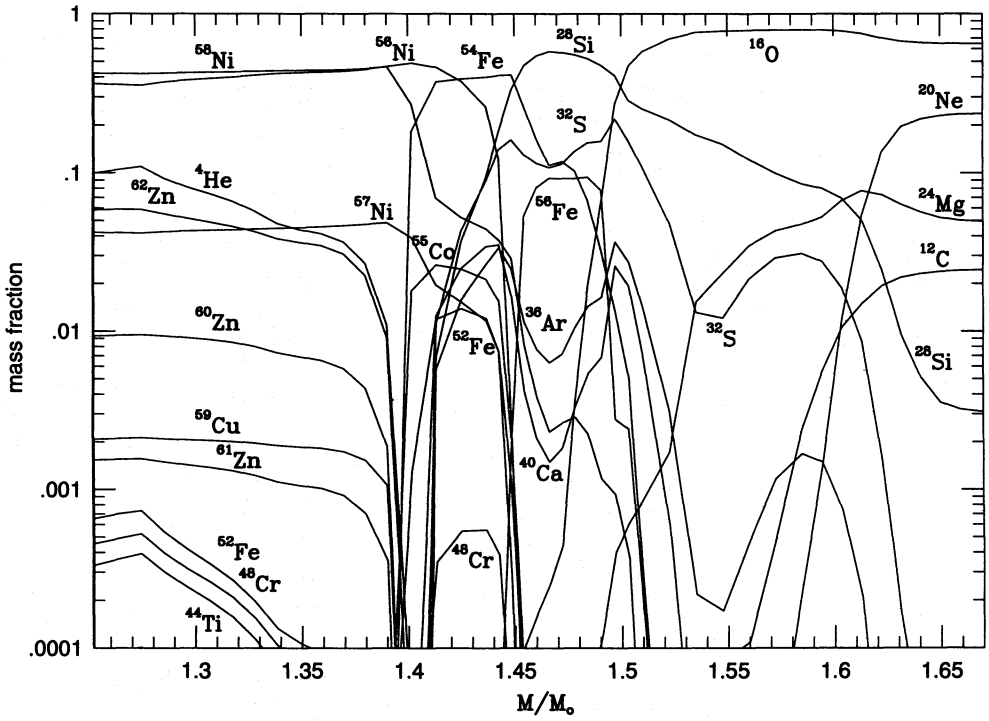

FIG. 1*b*

FIG. 1.—(*a–f*) The isotopic composition of the ejecta of core-collapse supernovae from 13, 15, 20, and 25 $M_\odot$ stars (3.3, 4, 6, and 8 $M_\odot$ He cores, respectively) is shown. Only the dominant abundances of intermediate-mass nuclei are plotted, while the Fe group composition is presented in full detail and its behavior is shown as a function of Y_e. The lower boundary of the $M(r)$ coordinate is not necessarily the mass cut between neutron star and ejecta. This depends on the details of the delayed explosion mechanism. (*a–b*) The 13 $M_\odot$ star and how strongly a Y_e change can affect the resulting composition are shown, making use of (*a*) a constant $Y_e = 0.4989$ in the inner ejecta and (*b*) the original Y_e resulting from the precollapse burning phases which drops to 0.4915. The ejecta composition for the 15 $M_\odot$ star with a constant $Y_e = 0.4988$ and a constant entropy in the innermost mass zones is shown in (*c*). Also displayed are the results for a 20 $M_\odot$ star with $Y_e = 0.4985$ in the innermost mass zones (*d*), or the original Y_e from the stellar model (*e*). Finally, the results for a 25 $M_\odot$ star are shown in (*f*). The choices of Y_e are taken from the solid and dashed lines in Figs. 2*a–2d*. For a detailed discussion, see the text.

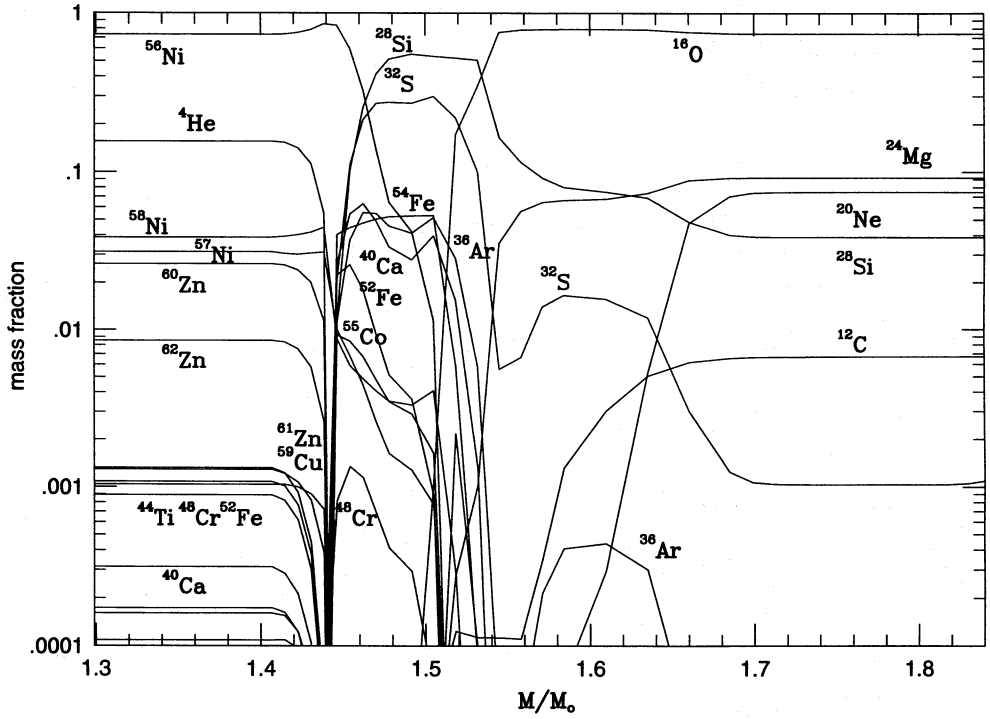

FIG. 1*c*

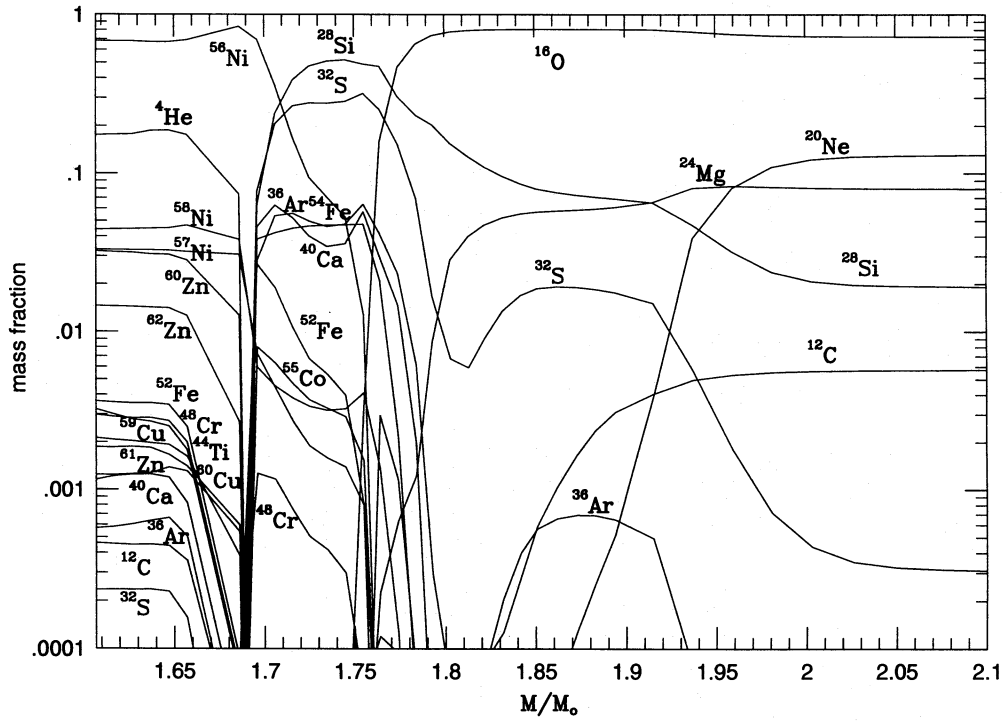

FIG. 1*d*

Figures 1*a* and 1*b* (both presenting the 13 $M_\odot$ star) make clear how strongly a Y_e change can affect the resulting composition. Figure 1*a* makes use of a constant $Y_e = 0.4989$ in the inner ejecta, experiencing incomplete and complete Si burning. Figure 1*b* makes use of the original Y_e resulting from the precollapse burning phases. Here Y_e drops to 0.4915 for mass zones below $M(r) = 1.5\ M_\odot$. Huge changes in the Fe-group composition can be noticed. Figure 1*c* shows the corresponding ejecta composition for the 15 $M_\odot$ star with a constant $Y_e = 0.4988$ and a constant entropy in the innermost mass zones (see discussion in § 3). Also shown are the results for a 20 $M_\odot$ star with $Y_e = 0.4985$ in the innermost mass zones (Fig. 1*d*), or the original Y_e from the stellar model (Fig. 1*e*). Finally, Figure 1*f* shows the results for a 25 $M_\odot$ star. A number of effects can be seen when comparing Figures 1*a* and 1*b*. The change in Y_e from 0.4989 to 0.4915 causes a tremendous change in the isotopic composition of the Fe group for the affected mass regions (< 1.5 $M_\odot$). In the latter case, the abundances of ^{58}Ni and ^{56}Ni become comparable. All neutron-rich isotopes increase

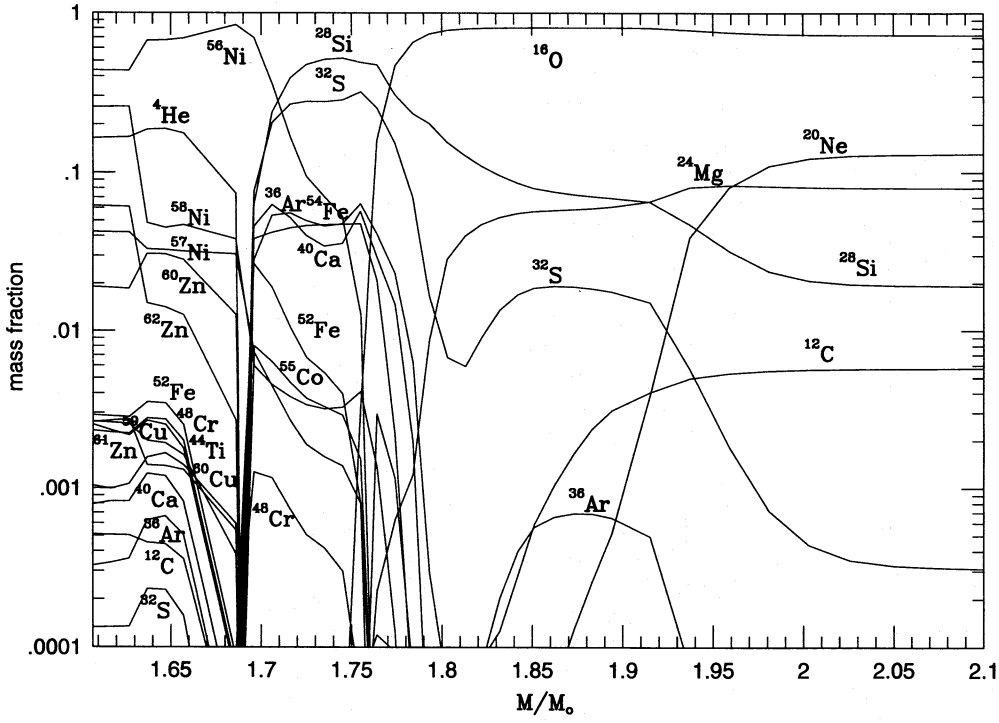

FIG. 1*e*

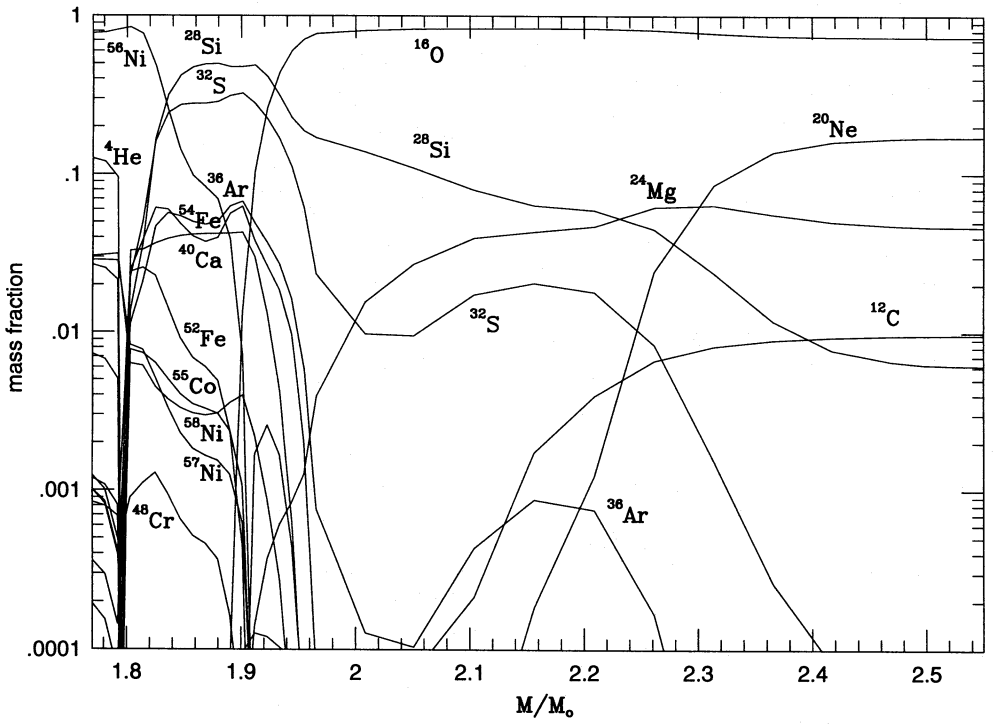

FIG. 1*f*

(^{57}Ni, ^{58}Ni, ^{59}Cu, ^{61}Zn, and ^{62}Zn), and the even-mass isotopes (^{58}Ni and ^{62}Zn) show the strongest effect. Figure 1*c* shows a very similar behavior as Figure 1*a*—both models possess the same Y_e—but there exists one difference, which is related to assuming a constant entropy in Figure 1*c*. In Figure 1*a*, one can recognize the increase of ^{40}Ca, ^{44}Ti, ^{48}Cr, and ^{52}Fe with an increasing remaining He mass fraction. These are direct consequences of an alpha-rich freezeout with increasing entropy, which will be discussed in more detail in § 3.1 and Figures 3 and 4*a*–4*b*. Figures 1*d* and 1*e* show a similar behavior as Figures 1*a*–1*b* for mass zones $<1.64\ M_\odot$, owing to the Y_e change, but somewhat reduced in scale. Y_e changes only moderately down to 0.494 rather than 0.4915.

Comparing Figures 1*a*–1*f* shows that the outer boundary of explosive Si burning with complete Si exhaustion is located for the four stellar models at 1.42, 1.46, 1.7, and 1.82 $M_\odot$, respectively. The latter number for the 25 $M_\odot$ star differs slightly from the estimates obtained in Table 1 with an explosion energy of 10^{51} ergs, while the hydrodynamic

calculation was performed with 1.5×10^{51} ergs because an appreciable gravitational binding energy has to be overcome for this massive star. Lifting the ejecta from the gravitational potential to obtain a similar kinetic energy as for the less massive supernova progenitors requires this enhanced explosion energy. When ejecting 0.15 $M_\odot$ and 0.13 $M_\odot$ of ^{56}Ni from the 13 and 15 $M_\odot$ stars, respectively, this would lead to mass cuts at 1.27 and 1.33 $M_\odot$ in case of explosive Si burning with small neutron excess $\eta = 1 - 2Y_e$ or large Y_e (>0.495). Amounts of 0.05 $M_\odot$ of ^{56}Ni for a 25 $M_\odot$ star seem to be consistent with chemical evolution models and, e.g., [O/Fe] and [Mg/Fe] ratios observable in low-metallicity stars (Tsujimoto et al. 1995). This corresponds to a mass cut at 1.77 $M_\odot$.

All these calculations were performed by depositing energy at a specific radius inside the Fe core and letting the shock wave propagate outward, which causes explosive burning. In reality, stellar models *at the time* t_{de}, *when the successful shock wave is initiated*, have to be utilized. Instead, they were taken at the onset of core collapse, which corresponds to a prompt explosion. Aufderheide et al. (1991) performed a calculation with a model at 0.29 s after core collapse for a 20 $M_\odot$ star, when the prompt shock had failed, and found an increase of the mass cut by roughly 0.02 $M_\odot$. A delayed explosion would set in after a delay of up to 1 s, with the exact time being somewhat uncertain and dependent on the details of neutrino transport.

As mentioned before, the outer boundary of explosive Si burning with Si exhaustion is the outer boundary of ^{56}Ni production. It was shown that this corresponds approximately to a radius $r_5 = 3700$ km for $T = 5 \times 10^9$ K and $E_{SN} \approx 10^{51}$ ergs. Therefore, the mass cut would be at

$$M_{cut} = M(r_5) - M_{ej}(^{56}\mathrm{Ni}) . \quad (2)$$

In case of a delayed explosion, we have to ask the question from which radius $r_{0,5}(t = 0)$ matter fell in, which is located at radius $r_5(t = t_{de}) = 3700$ km when the shock wave emerges at time t_{de}. Then the mass cut is not related to $M[r_5(0) = 3700\ \mathrm{km}]$ but to $M[r_5(t_{de}) = 3700\ \mathrm{km}] = M[r_{0,5}(0)]$ with

$$M_{cut} = M[r_{0,5}(0)] - M_{ej}(^{56}\mathrm{Ni})$$
$$= M[r_5(0) = 3700\ \mathrm{km}] + \Delta M_{acc} - M_{ej}(^{56}\mathrm{Ni}) . \quad (3)$$

When we assume a free-fall velocity and an attracting mass M inside the radius r_5, the time for infall is related to $r_5(t_{de})$ and $r_{0,5}(0)$ by

$$t_f = (2GM)^{-1/2} \int_{r_5}^{r_{0,5}} (1/r' - 1/r_{0,5})^{-1/2}\, dr' \quad (4)$$

(see Bethe 1990 and his eq. [6.37]). It is derived from energy conservation for a mass zone dm with $(1/2)dm(dr/dt)^2 = GM\, dm/r' - GM\, dm/r_{0,5}$. The solution given by Bethe is only valid for $r/r_{0,5} \ll 1$. Here we want to present the general result, based on the integral $\int r/(r_0 r - r^2)^{1/2}\, dr = -(r_0 r - r^2)^{1/2} - \arcsin[(-2r + r_0)/r_0]$ and relations for transcendental functions

$$t_f = (2GM)^{-1/2} r_{0,5}^{3/2} \left[\frac{1}{2} \arccos\left(\frac{2r}{r_{0,5}} - 1\right) + \sqrt{\frac{r}{r_{0,5}}\left(\frac{1-r}{r_{0,5}}\right)} \right] . \quad (5)$$

For typical core masses M, $(2GM)^{1/2}$ is of the order 2×10^{13} cm$^{3/2}$ s^{-1}, which we will take as a constant for all cores, because the square root has a weak mass dependence. Taking a timescale of 1 s for delayed explosions, this would lead to $r_{0,5}(0) = 6512$ km. This, however, neglects the sound travel time to $r_{0,5}$ before infall can set in. If r_s marks the location of the outmoving rarefaction wave at core bounce, the delay time consists of two parts

$$t_{de} = t_s(r_s, r_{0,5}) + t_f(r_{0,5}, r_5) \quad \text{with} \quad t_s = (r_{0,5} - r_s)/c_S \quad (6)$$

and has to be solved for $t_{de} \approx 1$ s. With a typical sound velocity $c_s = (\Gamma P/\rho)^{1/2}$ of 5000 km s^{-1} close to the Fe core, a sound wave would travel from $r_5 = 3700$ km to 6512 km within 0.56 s before any infall would have started. Therefore, we find $r_{0,5} \approx 5410$ km for a delay time of 1 s with $t_s \approx 0.34$ s and $t_f \approx 0.66$ s, approximating r_s by r_5. A delay time of 0.5 s corresponds accordingly to an $r_{0,5} \approx 4422$ km, $t_s \approx 0.14$ s, and $t_f \approx 0.36$ s, $t_{de} = 0.3$ s to $r_{0,5} \approx 4042$ km, $t_s \approx 0.07$ s, and $t_f \approx 0.23$ s. We can test the validity of this reasoning with a calculation we performed with a model taken at 0.29 s after bounce (Aufderheide et al. 1991). In that case, we find $\Delta M_{acc} \approx 0.02\ M_\odot$, consistent with the actual hydro calculation (see their Fig. 7).

In Figures 2*a*–2*d* we present the Y_e distributions of the four stellar models discussed here and the position of the outer boundary of explosive Si burning with complete Si exhaustion, M_{ex-Si}, as a function of the delay time t_{de}. We consider for each star delay times of 0, 0.3, 0.5, 1, and 2 s, resulting in $r_{0,5} = 3700$, 4042, 4412, 5410, and 7348 km. Inside this boundary, ^{56}Ni is produced as the dominant nucleus and the mass cuts would have to be positioned at $M_{cut} = M(r_{ex-Si}) - M(^{56}\mathrm{Ni}) = M[r_{0,5}(0)] - M(^{56}\mathrm{Ni})$. When Ni ejecta of 0.15, 0.13, 0.07, and 0.05 $M_\odot$ are used for the 13, 15, 20, and 25 $M_\odot$ stars, the mass cuts M_{cut} of Table 4 result for a vanishing delay time. For $t_{de} = 0.3$, 0.5, 1, and 2 s, the masses $\Delta M_{acc,i}$, $i = 1$, 2, 3, and 4 have to be added to M_{cut}. It is recognizable that especially for the 13 $M_\odot$ star the Y_e values encountered for these different delay times vary strongly, and differences of the Fe group composition can be expected. On the other extreme, the Y_e values in the innermost ejecta of the 25 $M_\odot$ star seem not to be affected at all by the available choices.

2.4. *Neutron Star Masses*

When taking into account the results of the previous section, we obtain baryonic neutron star masses M_b for the sequence of 13, 15, 20, and 25 $M_\odot$ SN II progenitors as noted in Table 4. Column (1) indicates the progenitor mass, column (2) gives the original Fe core mass, the absolute lower limit for M_b. The third column lists the outer boundary of explosive Si burning with Si exhausion M_{ex-Si}, which represents the outer edge of ^{56}Ni production when assuming a prompt explosion. The fourth column indicates

TABLE 4

MASS CUT IN SN II EVENTS

$M/M_\odot$	M_{core}	M_{Si-ex}	M_{cut}	ΔM_E	$\Delta M_{acc,1}$	$\Delta M_{acc,2}$	$\Delta M_{acc,3}$	$\Delta M_{acc,4}$
13	1.18	1.42	1.27	0.03	0.02	0.03	0.08	0.14
15	1.28	1.46	1.33	0.03	0.02	0.03	0.07	0.15
20	1.40	1.70	1.61	0.03	0.02	0.03	0.07	0.16
25	1.61	1.82	1.77	0.03	0.03	0.04	0.09	0.19

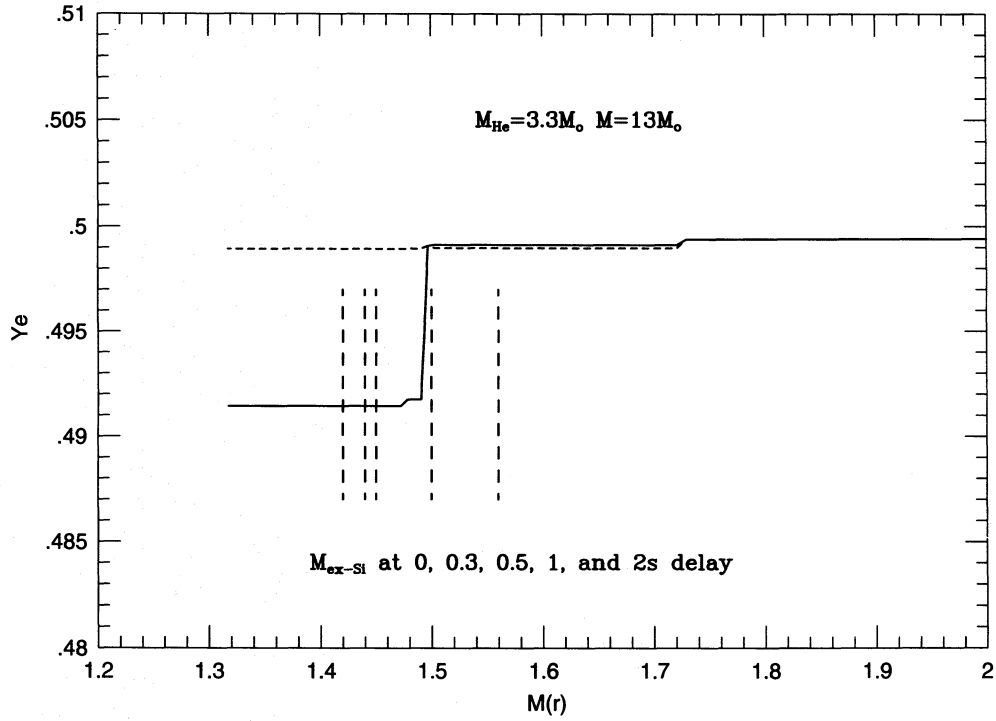

FIG. 2*a*

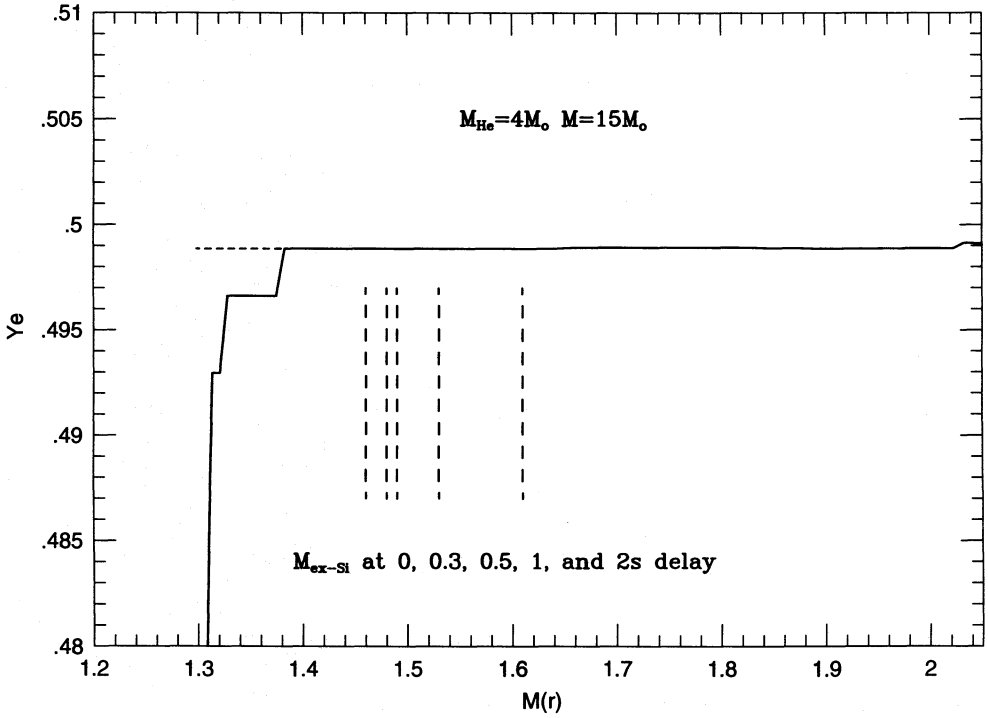

FIG. 2*b*

FIG. 2.—(*a–d*) The Y_e distributions of the four stellar models discussed and the position of the outer boundary of explosive Si burning with complete Si exhaustion, M_{ex-Si}, as a function of the delay/accretion period t_{de}. For each star, delay times of 0, 0.3, 0.5, 1, and 2 s are considered, resulting in $r_{0,5}$ = 3700, 4042, 4412, 5410, and 7348 km (see eqs. [3] and [4]). ^{56}Ni is produced inside this boundary $r_{0,5}$ as the dominant nucleus. For a given amount of Ni ejecta, mass cuts would have to be positioned at $M_{cut} = M(r_{ex-Si}) - M(^{56}\text{Ni}) = M[r_{0,5}(0)] - M(^{56}\text{Ni})$. The delay times t_{de} and required $M(^{56}\text{Ni})$ determine Y_e in the ejected material.

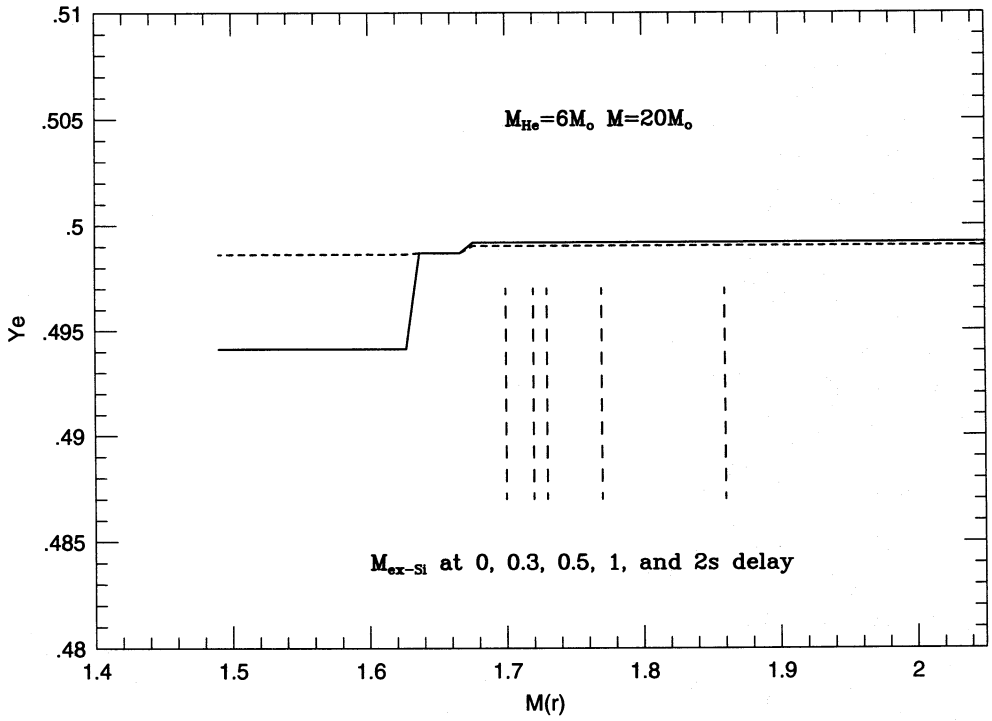

FIG. 2*c*

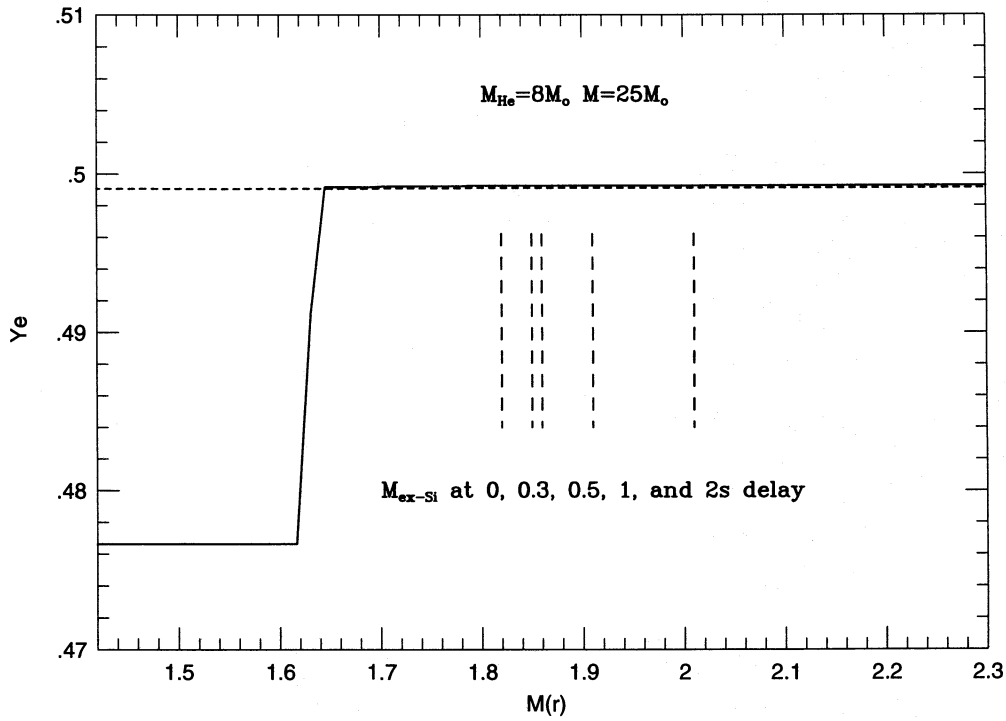

FIG. 2*d*

the location of the mass cut under the assumption that the amount of ^{56}Ni is ejected as required from light-curve and/or chemical evolution arguments, using equation (2), i.e., assuming a prompt explosion. In addition, one has to take into account the following error sources:

1. Y_e in the zones of explosive Si burning: A smaller Y_e leads to a reduction of the fraction of ^{56}Ni produced in this zone and could require a deeper mass cut and a smaller neutron star mass in order to fulfill the same constraint on the ejected amount of ^{56}Ni. A comparison of Figures 1*a* and 1*b*, with Y_e values at the inner boundary of 0.4989 and 0.4913, indicates the strong dependence.

2. Uncertainties in the explosion energy: The hydrodynamic calculations were performed under the assumption that the typical kinetic energy observed in supernova remnants is of the order 10^{51} ergs. This requires the deposition of a somewhat larger amount of energy inside the mass cut because some potential energy has to be overcome as well. The observed light curves for SN 1987A and SNe Ib/c

underline this finding. The radius r for a given temperature T is related to the explosion energy via the expanding radiation bubble (see eq. [1]), i.e., the radius at the outer boundary of complete Si burning with $T = 5 \times 10^9$ K (where only Fe group nuclei are produced) is proportional to $E^{1/3}$. We assume here that the deposited energy is uncertain by 50%. The neutron star mass cut moves with the mass boundary M_{ex-Si}. The resulting uncertainties are listed in column (5).

3. A final and probably the largest source of uncertainty is the still existing lack of a complete understanding of the SN II explosion mechanism. Utilizing precollapse models and depositing the correct explosion energy takes into account the philosophy of a prompt explosion. In case of a delayed explosion, accretion onto the proto–neutron star will occur until finally after a delay period t_{de} a shock wave is formed, leading to the ejection of the outer layers. The neutron star boundary would have to be moved outward accordingly. We estimate ΔM_{acc} in columns (6)–(9), the growth of the proto–neutron star by accretion for delay periods of 0.3, 0.5, 1, and 2 s, solving equations (3) and (6).

The previous discussion was related to the baryonic mass of the neutron star. The proto–neutron star with a baryonic mass M_b will release a binding energy E_{bin} in the form of blackbody radiation in neutrinos during its contraction to neutron star densities. This has been observed with the Kamiokande II and IMB detectors for SN 1987A (Hirata et al. 1987; Bionta et al. 1987; for a general discussion, see also Burrows 1990). The gravitational mass is then given by

$$M_g = M_b - E_{bin}/c^2 \, . \tag{7}$$

For reasonable uncertainties in the equation of state, Lattimer & Yahil (1989) obtained a relation between gravitational mass and binding energy

$$E_{bin} = (1.5 \pm 0.15)\left(\frac{M_g}{M_\odot}\right)^2 \times 10^{53} \text{ ergs} \, , \tag{8}$$

$$M_{bin} = \frac{E_{bin}}{c^2} = M_b - M_g$$

$$= (0.0839 \pm 0.0084)\left(\frac{M_g}{M_\odot}\right)^2 M_\odot \, . \tag{9}$$

Applying equation (9) results in a gravitational mass of the formed neutron star M_g as listed in columns (2), (3), (4), (5), and (6) of Table 5 for the corresponding progenitor masses and baryon masses of Table 4. An error of roughly $\pm 15\%$ for the difference $M_b - M_g$ applies. Here ΔM_{acc}, owing to the uncertainty of the accretion period or delay time, and the choice of $M(^{56}\text{Ni})$ from Table 3 which determines M_{cut} in Table 4, dominate the error in M_g. The lower bounds in column (2) correspond to prompt explosions. A delay time of about 1 s is expected to be an upper bound for the delayed explosions. This is close to a pure neutrino diffusion timescale without any convective turnover.

TABLE 5

NEUTRON STAR MASSES

$M/M_\odot$	M_g	$\Delta M_{g,acc,1}$	$\Delta M_{g,acc,2}$	$\Delta M_{g,acc,3}$	$\Delta M_{acc,4}$
13	1.16	0.01	0.02	0.06	0.11
15	1.21	0.01	0.02	0.06	0.12
20	1.45	0.01	0.02	0.06	0.12
25	1.56	0.03	0.04	0.08	0.19

It should first be noted that the discussion in this paper does not present straightforward results from detailed collapse and explosion calculations with completely understood physics of the explosion mechanism. It is based on the precollapse models from stellar evolution and constraints on the observed or required amount of ejected ^{56}Ni, which carries uncertainties of the order 0.05 $M_\odot$. We also did not make an attempt to quantify uncertainties entering the progenitor models. The numbers discussed for SN 1987A, where $M(^{56}\text{Ni})$ is well known, agree remarkably well with the ones obtained from the observed neutrino emission (Burrows 1990). A number of error sources have been taken into account, the largest being introduced by accretion of matter during a delayed explosion. The results indicate a clear spread of neutron star masses. This spread would be preserved in real supernova events, unless a conspiracy in the combination of proto–neutron star masses, delay times, and explosion energetics leads to a unique neutron star mass. Such a spread is also found in neutron star masses from observations (e.g., Nagase 1989; Page & Baron 1990; van Paradijs 1991), but it is not clear whether it is just a result of the large observational errors. We do not know whether the spread predicted in Table 5 already includes the uncertain upper mass limit of neutron stars owing to the nuclear equation of state (Baym 1991; Weber & Glendenning 1991). If it does, we would expect for these cases the formation of a central black hole during the delay period. Thus, no supernova explosion would occur and no yields would be ejected. Different maximum stable masses for the initially hot and a cold neutron star (see, e.g., Brown & Bethe 1994) could result in a supernova explosion and a central black hole.

3. DETAILED RESULTS

3.1. *The Results of Complete* Si *Burning*

The details of explosive nucleosynthesis in the individual mass zones of SNe II have been discussed, e.g., in Thielemann et al. (1990, 1994b) and should not be repeated here. Our concern in this paper is the question of whether theoretical predictions over a wider mass range of progenitor stars start to be safe, or whether any hidden uncertainties can flaw applications, e.g., for galactic chemical evolution calculations. For that reason, we will try to check any available comparisons with observational data. This will be done in § 4; here we present the detailed results, discuss some of the specifics, and explore a few features like the composition dependence on Y_e and entropy.

In the outer zones of ejected material, the composition after an SN II is only a function of (i) the stellar structure [$\rho(r)$, $T(r)$, $Y_i(r)$] alone (in unprocessed layers), or (ii) stellar structure and the shock strength, leading to an increase in ρ and T, which causes the explosive burning. In both cases, it does not matter how the shock originated. The results published in Thielemann et al. (1994b), which only discussed the zones of incomplete Si burning and those at larger radii, are an example of this type. In the innermost zones, a number of additional uncertainties enter. The composition is also a function of (iii) the delay time between collapse and explosion via neutrino heating (this will mostly determine the amount of accreted matter ΔM_{acc} and thus indirectly the Y_e at the mass cut). Also, very close to the shock formation region (the high-entropy bubble), (iv) the details of the shock formation can enter and affect densities

and temperatures in a different way than the passage of a mature shock. It is also here where one would expect deviations from a spherically symmetric treatment.

Some of the results were already shown and discussed in § 2.3 in Figures 1*a*–1*f*. In § 3.2 we will present the detailed isotopic composition of our explosion calculations, which reflect the influence of causes (i) and (ii) as a function of progenitor mass. We also will test cause (iii), the effect of the delay time or Y_e on the composition, by correcting Y_e according to accretion during the delay period t_{de} between the collapse and explosion. Before presenting the detailed results and their dependence on cause (iv), we want to explore in this subsection possible effects of the shock formation on density or temperature by analyzing the nucleosynthesis as a function of entropy. This feature was not discussed in § 2.

It turns out that at the high temperatures in the innermost zones, at which pressure and entropy are radiation dominated [$P_\gamma = aT^4/3$, $S_\gamma = (4/3)aT^3/\rho$; radiation entropy per gram of matter], the radiation entropy is a good measure of temperature and density. We know that in complete Si burning at low densities, one obtains an alpha-rich freezeout. This is attributable to the inability of the triple-α and other reactions to bridge the $A = 5$ and 8 gaps of stable nuclei during the expansion and quasi-adiabatic cooling to lower temperatures when neutrons, protons, and alpha particles reassemble to form heavier nuclei. This effect increases for higher peak temperatures and for lower densities because of the strong density dependence of the three-body reactions involved. Figure 3 shows that the remaining alpha fraction in an alpha-rich freezeout is well described as a function of radiation entropy. Different combinations of ρ and T, leading to the same S_γ, give identical results for X_α within numerical uncertainties. The calculations were performed for $Y_e = 0.4989$. An entropy dependence of the alpha-rich freezeout is also well observed in Figure 1*a*. When comparing Figures 1*a* and 1*b*, we see a Y_e dependence. Lower Y_e values lead to a less pronounced alpha-rich freezeout because three-body reactions involving neutrons like ^{4}He(αn, γ)^{9}Be help to bridge the $A = 5$ and 8 gaps, competing with and enhancing the effect of the triple-α reaction. Figures 4*a* and 4*b* show the resulting composition up to Cr and from Mn to Ni (after decay) as a function of remaining X_α. One can recognize that the lighter nuclei, being produced by alpha captures from a remaining alpha reservoir, have larger abundances for more pronounced alpha-rich freezeouts with larger remaining alpha fractions. The same is true for nuclei beyond Fe and Ni because alpha capture from the dominant Fe group nuclei increases their abundances. Logically, only the dominant Fe group nuclei like Fe and Ni decrease in abundance for larger remaining alpha fractions.

3.2. *Isotopic Yields for the 13, 15, 20, and 25 $M_\odot$ Models*

Detailed explosive nucleosynthesis calculations for progenitors of 13, 15, and 25 $M_\odot$ were performed in the same way as in Hashimoto et al. (1989) and Thielemann et al. (1990) for the 20 $M_\odot$ star. For first results, see Thielemann et al. (1994b) and Hashimoto et al. (1993b). Figures 1*a*–1*f* gave an idea of how the explosive and hydrostatic burning zones are distributed as a function of the Lagrangian mass coordinate. One can recognize how, with increasing progenitor mass, the appropriate explosive and hydrostatic burning zones also appear at larger mass coordinates. They can also be compared with the analytical estimates in Table 1 and are in good agreement. At present, no proven evi-

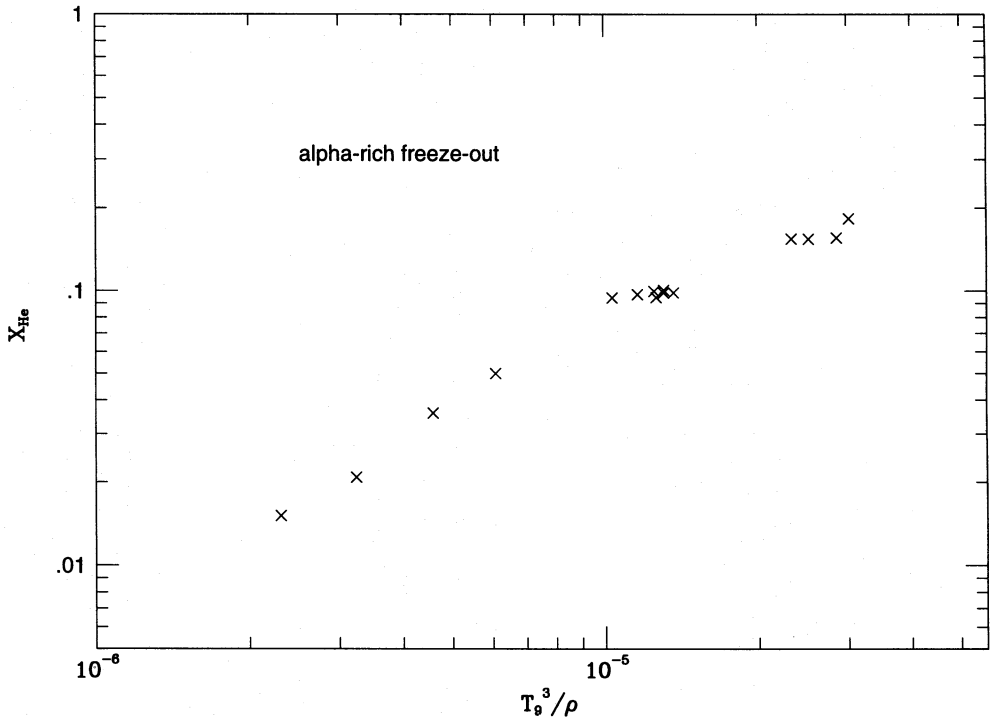

FIG. 3.—Complete Si burning at low densities leads to an alpha-rich freezeout, owing to the inability of the triple-α and other reactions to bridge the $A = 5$ and 8 gaps of stable nuclei. The effect increases for higher peak temperatures and for lower densities because of the strong density dependence of the three-body reactions involved. The remaining alpha fraction X_α is plotted as a funcion of the radiation entropy $S_\gamma = (4/3)aT^3/\rho$. Different combinations of ρ and T produce identical X_α for the same S_γ. The results are dependent on Y_e, here we used $Y_e = 0.4988$.

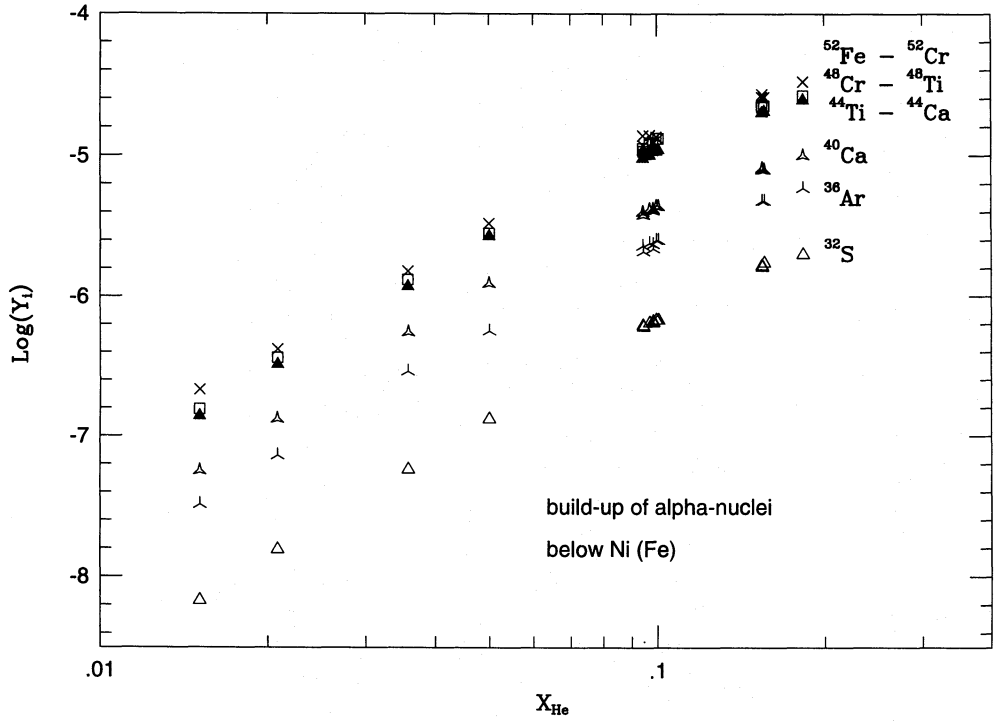

FIG. 4*a*

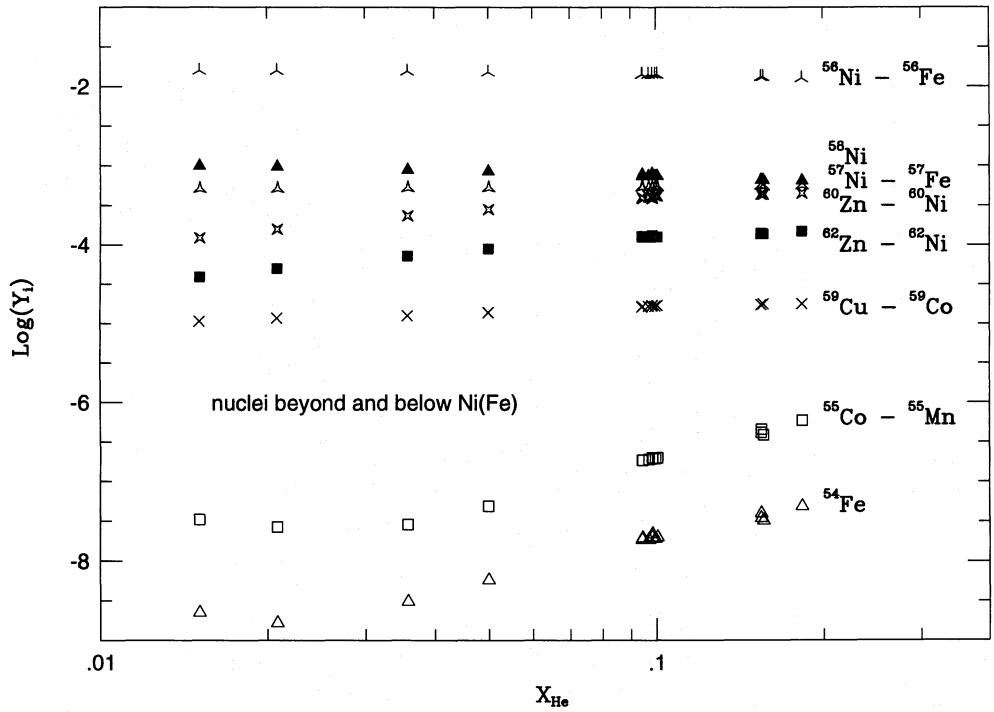

FIG. 4*b*

FIG. 4.—(*a*, *b*) The composition up to Cr and from Mn to Ni (after decay) as a function of the remaining alpha fraction X_α. Lighter nuclei, being produced by alpha captures from a remaining alpha reservoir, have larger abundances for more pronounced alpha-rich freezeouts with larger X_α. Nuclei beyond Fe and Ni behave similarly because of alpha captures starting from the dominant Fe-group nuclei. Therefore, the dominant Fe group nuclei like Fe and Ni show the opposite behavior.

dence about the position of the mass cut between neutron star and ejecta exists in these cases. Therefore, we made a number of choices, based on the expected ^{56}Ni ejecta discussed in § 2 and Y_e distributions corresponding to different delay times and accretion periods. Tables 6 through 13 list the integrated abundances with the choices given in each table heading.

Tables 6A–6B give the results for the 13 $M_\odot$ star; Table 6A assumes $Y_e = 0.4989$ also for the mass zones with $M(r) < 1.5\ M_\odot$, which corresponds to Figure 1*a* and the dashed line in Figure 2*a*. Table 6B makes use of the original Y_e, shown as the solid line in Figure 2*a*, which corresponds to the composition of Figure 1*b*. Table 7 displays the results for the 15 $M_\odot$ star, assuming a $Y_e = 0.4988$ as shown by the

TABLE 6A

COMPOSITION OF EJECTA $M = 13\ M_\odot$, Y_e = CONSTANT

	M/M⊙		M/M⊙		M/M⊙		M/M⊙		M/M⊙
d	2.62E-27	t	2.82E-19	he3	7.33E-19	he4	1.46E+00	li7	1.67E-25
be10	3.83E-24	b10	3.62E-23	b11	4.25E-14	b12	4.36E-25	c11	9.93E-18
c12	5.94E-02	c13	6.23E-09	c14	6.70E-09	n13	1.57E-12	n14	6.09E-03
n15	2.65E-08	n16	9.62E-22	n17	7.40E-23	o14	1.52E-17	o15	1.20E-11
o16	2.05E-01	o17	6.44E-08	o18	1.01E-02	o19	1.12E-15	o20	5.45E-18
f17	1.69E-19	f18	1.36E-10	f19	9.40E-10	f20	1.02E-11	f21	4.37E-13
ne18	5.25E-22	ne19	5.70E-16	ne20	2.49E-02	ne21	2.31E-04	ne22	2.92E-03
ne23	3.72E-09	ne24	4.70E-13	ne25	3.93E-20	na21	2.46E-14	na22	9.84E-08
na23	8.03E-04	na24	2.84E-06	na25	1.03E-08	na26	1.58E-12	mg22	8.09E-17
mg23	9.25E-07	mg24	9.63E-03	mg25	1.50E-03	mg26	1.02E-03	mg27	1.82E-07
mg28	1.03E-09	al24	9.13E-20	al25	7.38E-12	al26	1.82E-06	al27	1.08E-03
al28	1.01E-05	al29	1.40E-07	al30	7.87E-11	si26	1.64E-13	si27	5.47E-07
si28	4.77E-02	si29	6.52E-04	si30	1.41E-03	si31	1.65E-06	si32	1.32E-08
si33	9.79E-15	p27	7.33E-26	p28	3.87E-19	p29	1.33E-10	p30	1.25E-06
p31	2.37E-04	p32	4.60E-07	p33	2.92E-07	p34	1.40E-10	p35	3.30E-12
s29	6.77E-23	s30	2.53E-13	s31	8.57E-08	s32	2.36E-02	s33	1.05E-04
s34	1.36E-03	s35	2.73E-07	s36	2.91E-07	s37	4.45E-15	s38	3.50E-16
cl32	1.33E-17	cl33	1.65E-11	cl34	3.46E-08	cl35	3.78E-05	cl36	5.01E-07
cl37	6.63E-07	cl38	5.95E-11	cl39	2.87E-12	cl40	1.24E-15	ar33	3.05E-20
ar34	5.94E-12	ar35	1.16E-07	ar36	4.45E-03	ar37	8.39E-06	ar38	4.90E-04
ar39	3.45E-09	ar40	3.68E-09	ar41	5.45E-12	ar42	3.05E-13	ar43	2.12E-16
ar44	1.23E-17	k36	3.19E-15	k37	5.47E-12	k38	8.75E-08	k39	2.64E-05
k40	1.02E-08	k41	3.28E-09	k42	1.04E-10	k43	1.83E-11	k44	1.93E-12
k45	5.42E-13	k46	1.29E-14	ca37	8.73E-19	ca38	4.03E-12	ca39	7.11E-07
ca40	4.25E-03	ca41	2.29E-06	ca42	1.28E-05	ca43	1.46E-08	ca44	1.01E-08
ca45	3.49E-11	ca46	3.21E-11	ca47	1.92E-12	ca48	9.77E-14	ca49	4.38E-19
sc40	3.90E-19	sc41	8.13E-15	sc42	5.82E-08	sc43	5.21E-07	sc44	8.10E-10
sc45	4.64E-09	sc46	1.27E-10	sc47	3.92E-11	sc48	6.08E-12	sc49	6.24E-13
sc50	1.76E-16	ti42	1.65E-16	ti43	3.90E-07	ti44	5.56E-05	ti45	7.59E-08
ti46	4.88E-06	ti47	9.61E-08	ti48	4.85E-08	ti49	1.80E-10	ti50	1.15E-10
ti51	2.93E-14	ti52	9.79E-15	v44	2.97E-14	v45	9.08E-12	v46	1.16E-08
v47	1.75E-06	v48	1.52E-08	v49	3.19E-08	v50	5.05E-10	v51	3.64E-09
v52	5.00E-13	v53	1.12E-13	v54	1.58E-17	cr46	4.15E-11	cr47	1.79E-06
cr48	1.36E-04	cr49	5.49E-06	cr50	4.50E-05	cr51	7.15E-07	cr52	7.47E-06
cr53	1.92E-09	cr54	5.91E-11	cr55	2.18E-16	cr56	2.41E-16	mn48	7.26E-13
mn49	3.31E-10	mn50	2.33E-08	mn51	1.06E-05	mn52	2.41E-07	mn53	4.39E-06
mn54	2.28E-08	mn55	8.12E-09	mn56	3.59E-14	mn57	1.68E-15	mn58	2.06E-18
fe50	1.27E-12	fe51	4.47E-07	fe52	1.42E-03	fe53	1.35E-04	fe54	4.32E-03
fe55	2.08E-05	fe56	5.71E-05	fe57	7.45E-09	fe58	4.11E-10	fe59	1.42E-16
fe60	1.80E-17	fe61	7.14E-22	fe62	4.08E-21	co52	7.84E-16	co53	5.89E-12
co54	1.43E-07	co55	5.48E-04	co56	3.87E-06	co57	2.91E-06	co58	7.94E-09
co59	3.55E-09	co60	6.31E-14	co61	5.37E-16	co62	7.52E-20	co63	3.42E-19
ni54	1.16E-14	ni55	1.66E-07	ni56	1.53E-01	ni57	4.59E-03	ni58	6.07E-03
ni59	1.76E-06	ni60	2.25E-06	ni61	6.50E-10	ni62	2.92E-10	ni63	5.49E-16
ni64	2.21E-17	ni65	3.97E-22	ni66	2.90E-21	ni67	2.69E-25	cu57	7.45E-13
cu58	5.38E-07	cu59	1.24E-04	cu60	1.20E-05	cu61	7.47E-07	cu62	3.47E-08
cu63	1.07E-10	cu64	9.37E-16	cu65	1.31E-16	cu66	1.92E-21	cu67	1.15E-20
cu68	7.66E-24	cu69	1.08E-22	zn59	3.00E-11	zn60	3.13E-03	zn61	1.38E-04
zn62	9.29E-04	zn63	3.66E-07	zn64	3.95E-09	zn65	7.07E-12	zn66	1.51E-13
zn67	1.15E-17	zn68	6.34E-20	zn69	7.27E-24	zn70	1.07E-22	zn72	1.11E-24
ga61	7.39E-15	ga62	2.58E-09	ga63	4.24E-07	ga64	1.54E-07	ga65	1.24E-08
ga66	1.73E-09	ga67	8.36E-12	ga68	1.96E-16	ga69	8.57E-18	ga70	3.89E-23
ga71	3.60E-23	ga72	2.24E-25	ga73	5.72E-24	ge63	2.51E-13	ge64	1.41E-05
ge65	6.68E-07	ge66	1.38E-05	ge67	1.47E-08	ge68	4.89E-09	ge69	3.64E-13
ge70	2.97E-15	ge71	7.17E-20	ge72	6.03E-23	ge74	2.93E-25	ge76	1.87E-25

TABLE 6B

COMPOSITION OF EJECTA $M = 13\ M_\odot$, ORIGINAL Y_e

	M/M⊙		M/M⊙		M/M⊙		M/M⊙		M/M⊙
t	2.82E-19	he3	7.33E-19	he4	1.46E+00	li7	1.67E-25	be10	3.97E-24
b10	3.62E-23	b11	4.25E-14	b12	4.36E-25	c11	9.01E-18	c12	5.94E-02
c13	6.23E-09	c14	6.70E-09	n13	8.67E-14	n14	6.09E-03	n15	2.65E-08
n16	9.62E-22	n17	7.40E-23	o14	1.88E-19	o15	8.78E-12	o16	2.05E-01
o17	6.44E-08	o18	1.01E-02	o19	1.12E-15	o20	5.45E-18	f17	9.88E-20
f18	1.36E-10	f19	9.40E-10	f20	1.02E-11	f21	4.37E-13	ne18	4.36E-24
ne19	5.70E-16	ne20	2.49E-02	ne21	2.31E-04	ne22	2.92E-03	ne23	3.72E-09
ne24	4.70E-13	ne25	3.93E-20	na21	9.65E-15	na22	9.84E-08	na23	8.03E-04
na24	2.84E-06	na25	1.03E-08	na26	1.58E-12	mg22	7.75E-17	mg23	9.24E-07
mg24	9.63E-03	mg25	1.50E-03	mg26	1.02E-03	mg27	1.82E-07	mg28	1.03E-09
al24	9.13E-20	al25	2.46E-13	al26	1.82E-06	al27	1.08E-03	al28	1.01E-05
al29	1.40E-07	al30	7.87E-11	si26	1.55E-13	si27	5.46E-07	si28	4.66E-02
si29	6.96E-04	si30	1.50E-03	si31	1.65E-06	si32	1.32E-08	si33	9.79E-15
p28	2.45E-19	p29	4.21E-12	p30	1.20E-06	p31	2.81E-04	p32	4.67E-07
p33	2.95E-07	p34	1.40E-10	p35	3.30E-12	s29	8.53E-25	s30	5.86E-15
s31	1.99E-08	s32	1.46E-02	s33	1.48E-04	s34	2.43E-03	s35	2.78E-07
s36	2.91E-07	s37	4.45E-15	s38	3.50E-16	cl32	1.00E-19	cl33	5.09E-13
cl34	1.64E-08	cl35	5.98E-05	cl36	5.49E-07	cl37	7.40E-07	cl38	5.95E-11
cl39	2.87E-12	cl40	1.24E-15	ar33	4.06E-23	ar34	8.86E-14	ar35	1.98E-08
ar36	1.93E-03	ar37	1.26E-05	ar38	1.15E-03	ar39	4.21E-09	ar40	3.83E-09
ar41	5.45E-12	ar42	3.05E-13	ar43	2.12E-16	ar44	1.23E-17	k36	3.68E-17
k37	1.00E-13	k38	5.73E-08	k39	3.82E-05	k40	1.41E-08	k41	4.43E-09
k42	1.04E-10	k43	1.83E-11	k44	1.93E-12	k45	5.42E-13	k46	1.29E-14
ca37	9.69E-22	ca38	5.47E-14	ca39	3.04E-07	ca40	1.57E-03	ca41	2.82E-06
ca42	2.57E-05	ca43	3.12E-08	ca44	1.98E-08	ca45	3.61E-11	ca46	3.23E-11
ca47	1.92E-12	ca48	9.77E-14	ca49	4.38E-19	sc40	1.21E-20	sc41	2.06E-16
sc42	1.92E-08	sc43	1.43E-07	sc44	1.80E-09	sc45	1.08E-08	sc46	1.61E-10
sc47	5.24E-11	sc48	6.09E-12	sc49	6.24E-13	sc50	1.76E-16	ti42	2.25E-18
ti43	2.20E-08	ti44	2.40E-05	ti45	9.84E-08	ti46	1.19E-05	ti47	3.70E-07
ti48	1.32E-06	ti49	2.22E-09	ti50	3.49E-09	ti51	2.96E-14	ti52	9.79E-15
v44	1.18E-16	v45	2.79E-13	v46	4.56E-08	v47	1.58E-06	v48	3.33E-08
v49	6.84E-07	v50	2.18E-08	v51	2.25E-07	v52	2.50E-12	v53	1.13E-13
v54	1.58E-17	cr46	7.30E-13	cr47	1.44E-06	cr48	4.91E-05	cr49	4.85E-06
cr50	3.35E-04	cr51	2.29E-05	cr52	1.25E-03	cr53	4.92E-07	cr54	2.46E-08
cr55	1.23E-15	cr56	2.41E-16	mn48	4.18E-14	mn49	1.02E-11	mn50	1.11E-07
mn51	1.54E-05	mn52	1.37E-06	mn53	2.30E-04	mn54	2.59E-06	mn55	1.50E-06
mn56	6.90E-12	mn57	1.44E-14	mn58	2.06E-18	fe50	2.55E-14	fe51	2.40E-07
fe52	5.11E-04	fe53	1.51E-04	fe54	2.46E-02	fe55	5.57E-04	fe56	3.58E-03
fe57	7.90E-07	fe58	9.45E-08	fe59	3.23E-14	fe60	1.82E-16	fe61	7.14E-22
fe62	4.08E-21	co52	3.08E-17	co53	1.94E-13	co54	1.93E-07	co55	1.10E-03
co56	1.67E-05	co57	5.24E-05	co58	2.86E-07	co59	2.93E-07	co60	7.36E-12
co61	1.91E-13	co62	1.09E-19	co63	3.43E-19	ni54	2.41E-16	ni55	3.22E-08
ni56	7.65E-02	ni57	7.37E-03	ni58	6.77E-02	ni59	2.15E-05	ni60	7.25E-05
ni61	3.57E-08	ni62	3.64E-08	ni63	9.24E-14	ni64	1.04E-14	ni65	7.60E-22
ni66	2.91E-21	ni67	2.69E-25	cu57	2.12E-14	cu58	8.96E-08	cu59	2.69E-04
cu60	9.83E-06	cu61	3.32E-06	cu62	3.60E-07	cu63	3.87E-09	cu64	7.18E-14
cu65	2.56E-14	cu66	5.23E-20	cu67	1.45E-20	cu68	7.66E-24	cu69	1.08E-22
zn59	8.94E-13	zn60	1.07E-03	zn61	1.69E-04	zn62	6.01E-03	zn63	9.78E-06
zn64	1.02E-06	zn65	3.67E-10	zn66	4.39E-12	zn67	3.66E-16	zn68	1.50E-17
zn69	8.99E-24	zn70	1.07E-22	zn72	1.11E-24	ga61	1.64E-16	ga62	3.81E-10
ga63	4.21E-07	ga64	3.68E-07	ga65	1.81E-07	ga66	1.40E-08	ga67	1.53E-10
ga68	2.39E-14	ga69	2.67E-15	ga70	2.30E-20	ga71	1.08E-22	ga72	2.24E-25
ga73	5.72E-24	ge63	5.05E-15	ge64	2.91E-06	ge65	6.13E-07	ge66	6.91E-05
ge67	1.96E-07	ge68	3.38E-07	ge69	5.92E-11	ge70	3.65E-12	ge71	1.72E-16
ge72	1.92E-19	ge74	2.93E-25	ge76	1.87E-25				

TABLE 7

COMPOSITION OF EJECTA $M = 15\ M_\odot$

	M/M$_\odot$		M/M$_\odot$		M/M$_\odot$		M/M$_\odot$		M/M$_\odot$
d	3.03E-26	t	1.51E-20	he3	6.90E-20	he4	1.83E+00	be10	7.45E-25
b10	5.73E-24	b11	2.02E-15	c11	1.27E-17	c12	8.33E-02	c13	4.95E-10
c14	1.93E-10	n13	2.73E-12	n14	5.37E-03	n15	1.52E-10	o14	3.87E-17
o15	5.73E-12	o16	4.23E-01	o17	5.08E-09	o18	1.35E-02	o19	3.96E-19
o20	2.10E-21	f17	4.73E-19	f18	2.97E-11	f19	2.67E-11	f20	4.78E-14
f21	1.88E-15	ne18	1.25E-21	ne19	1.40E-16	ne20	2.83E-02	ne21	4.53E-05
ne22	1.26E-02	ne23	1.24E-10	ne24	1.02E-15	ne25	4.13E-24	na21	3.53E-14
na22	3.98E-08	na23	2.08E-04	na24	3.14E-08	na25	1.89E-11	na26	3.53E-16
mg22	4.22E-17	mg23	5.36E-07	mg24	4.20E-02	mg25	3.46E-03	mg26	2.52E-03
mg27	1.95E-08	mg28	1.87E-11	al24	9.82E-21	al25	1.49E-11	al26	2.68E-06
al27	5.55E-03	al28	6.72E-06	al29	1.82E-08	al30	1.08E-12	si26	5.47E-14
si27	1.06E-06	si28	6.52E-02	si29	4.40E-03	si30	4.91E-03	si31	2.91E-06
si32	7.65E-09	si33	2.91E-16	p27	6.90E-25	p28	3.85E-19	p29	2.83E-10
p30	1.66E-06	p31	8.64E-04	p32	9.71E-07	p33	5.34E-07	p34	6.07E-11
p35	2.89E-13	s29	7.38E-23	s30	4.25E-13	s31	7.07E-08	s32	2.16E-02
s33	9.26E-05	s34	1.09E-03	s35	6.07E-07	s36	5.27E-07	s37	9.28E-16
s38	4.92E-17	cl32	2.39E-17	cl33	3.35E-11	cl34	3.55E-08	cl35	5.40E-05
cl36	5.81E-07	cl37	6.78E-07	cl38	2.56E-11	cl39	4.54E-13	cl40	4.03E-17
ar33	6.49E-20	ar34	7.30E-12	ar35	1.45E-07	ar36	3.49E-03	ar37	4.94E-06
ar38	3.26E-04	ar39	3.02E-09	ar40	4.12E-09	ar41	1.21E-12	ar42	3.04E-14
ar43	3.95E-18	ar44	4.09E-20	k36	5.32E-15	k37	1.05E-11	k38	1.17E-07
k39	1.62E-05	k40	7.04E-09	k41	2.64E-09	k42	4.08E-11	k43	2.67E-12
k44	5.58E-14	k45	3.45E-15	k46	2.04E-17	ca37	2.08E-18	ca38	4.88E-12
ca39	9.22E-07	ca40	3.03E-03	ca41	1.25E-06	ca42	6.90E-06	ca43	5.78E-09
ca44	4.27E-09	ca45	7.55E-12	ca46	8.50E-12	ca47	3.02E-14	ca48	6.71E-16
ca49	2.42E-22	sc40	7.21E-19	sc41	1.57E-14	sc42	7.82E-08	sc43	7.28E-07
sc44	4.68E-10	sc45	1.86E-09	sc46	4.60E-11	sc47	1.22E-11	sc48	2.96E-13
sc49	1.20E-14	sc50	1.45E-19	ti42	2.10E-16	ti43	4.72E-07	ti44	7.19E-05
ti45	4.47E-08	ti46	2.70E-06	ti47	5.00E-08	ti48	3.43E-08	ti49	2.18E-10
ti50	4.59E-10	ti51	5.51E-16	ti52	2.48E-18	v44	4.67E-14	v45	1.57E-11
v46	1.51E-08	v47	2.42E-06	v48	8.54E-09	v49	1.70E-08	v50	3.51E-10
v51	2.79E-09	v52	1.11E-13	v53	7.81E-16	v54	4.43E-21	cr46	4.29E-11
cr47	2.20E-06	cr48	1.27E-04	cr49	4.13E-06	cr50	3.85E-05	cr51	3.79E-07
cr52	6.08E-06	cr53	1.95E-09	cr54	1.11E-10	cr55	3.16E-17	cr56	1.31E-19
mn48	1.05E-12	mn49	5.34E-10	mn50	2.75E-08	mn51	9.21E-06	mn52	1.64E-07
mn53	2.04E-06	mn54	1.54E-08	mn55	6.84E-09	mn56	4.10E-14	mn57	2.27E-16
mn58	5.37E-22	fe50	1.15E-12	fe51	4.87E-07	fe52	8.18E-04	fe53	8.72E-05
fe54	3.51E-03	fe55	7.92E-06	fe56	3.04E-05	fe57	4.90E-09	fe58	3.82E-10
fe59	3.73E-16	fe60	1.25E-17	fe61	3.67E-24	fe62	1.24E-24	co52	1.11E-15
co53	8.81E-12	co54	1.66E-07	co55	3.31E-04	co56	3.93E-06	co57	1.24E-06
co58	3.24E-09	co59	1.95E-09	co60	4.14E-14	co61	2.47E-15	co62	2.20E-20
co63	2.63E-20	ni54	1.00E-14	ni55	1.72E-07	ni56	1.30E-01	ni57	4.64E-03
ni58	6.64E-03	ni59	1.50E-06	ni60	9.52E-07	ni61	3.38E-10	ni62	2.10E-10
ni63	9.01E-16	ni64	9.17E-16	ni65	1.87E-21	ni66	7.06E-21	cu57	8.94E-13
cu58	6.42E-07	cu59	1.34E-04	cu60	1.33E-05	cu61	8.75E-07	cu62	5.25E-08
cu63	1.61E-10	cu64	6.52E-16	cu65	8.87E-16	cu66	6.46E-20	cu67	6.28E-19
cu68	5.79E-24	cu69	8.11E-24	zn59	3.67E-11	zn60	3.12E-03	zn61	1.45E-04
zn62	1.00E-03	zn63	4.62E-07	zn64	4.88E-09	zn65	1.05E-11	zn66	3.30E-13
zn67	2.68E-17	zn68	9.65E-18	zn69	1.21E-22	zn70	3.19E-21	ga61	9.79E-15
ga62	2.76E-09	ga63	4.94E-07	ga64	1.75E-07	ga65	1.52E-08	ga66	2.53E-09
ga67	1.39E-11	ga68	3.70E-16	ga69	2.37E-17	ga70	7.48E-22	ga71	2.29E-20
ga72	1.69E-24	ga73	6.03E-23	ge63	3.25E-13	ge64	1.39E-05	ge65	7.54E-07
ge66	1.47E-05	ge67	1.94E-08	ge68	6.35E-09	ge69	6.47E-13	ge70	5.13E-15
ge71	1.82E-19	ge72	5.57E-20	ge73	1.65E-23	ge74	1.12E-21	ge76	4.37E-24

dashed line of Figure 2*b*. Tables 8A and 8B give the results for the 20 $M_\odot$ star; Table 8A utilizes a $Y_e = 0.4985$ in the inner ejected mass zones, which corresponds to the dashed line in Figure 2*c*. Table 8B makes use of the original Y_e, which features a decrease down to 0.494. Tables 8A and 8B correspond to Figures 1*d* and 1*e*. Table 9 presents the yields of the 25 $M_\odot$ star. There is no uncertainty involved for the Y_e in the inner mass zones, as Figure 2*d* indicates. Therefore, the original Y_e was chosen. Table 9 corresponds to Figure 1*f*. It should be noted at this point that owing to a restricted nucleosynthesis treatment during hydrostatic evolution, the given ^{26}Al yields only represent the fraction which is produced explosively. The latter can only be a lower limit to the actual ^{26}Al ejected and should be taken with care for the purpose of studying isotopic anomalies or the total SNe II ^{26}Al production in the Galaxy.

The mass cuts chosen in these models are, of course, uncertain, as is apparent from the discussion in § 2.2. We made the choice based on the discussion in § 2 which results in 0.15, 0.13, 0.075, and 0.05 $M_\odot$ of ^{56}Ni ejected for the versions of each stellar model utilizing the Y_e from the dashed lines in Figures 2*a*–2*d*. Should future observational constraints and/or self-consistent models require different Ni ejecta, like a relatively weak progenitor mass dependence with typical values in the uncertainty range 0.07–0.1 $M_\odot$, the results presented here have to be adjusted. In that case, we suggest to scale all products of the Fe group from Cr to Zn plus ^{44}Ti with the same adjustment factor as ^{56}Ni. ^{54}Fe and ^{55}Co should be excluded from this procedure, as they are produced dominantly in incomplete Si burning, which is not affected by the mass cut, as can be seen from Figures 1*a*–1*f*. One can also recognize from these figures

TABLE 8A

COMPOSITION OF EJECTA $M = 20\ M_\odot$

	M/M⊙		M/M⊙		M/M⊙		M/M⊙		M/M⊙
d	4.05E-17	t	6.17E-20	he3	2.50E-19	he4	2.10E+00	li6	6.09E-19
li7	5.40E-20	be7	5.56E-22	be9	8.21E-18	be10	1.52E-21	b10	3.24E-17
b11	1.04E-14	b12	6.12E-24	c11	1.25E-17	c12	1.14E-01	c13	4.86E-07
c14	1.00E-08	c15	1.87E-14	n13	8.19E-11	n14	2.71E-03	n15	5.06E-08
n16	5.53E-13	n17	1.38E-18	o14	3.60E-18	o15	1.48E-11	o16	1.48E+00
o17	1.84E-08	o18	8.68E-03	o19	8.07E-10	o20	1.78E-13	f17	5.35E-15
f18	2.37E-08	f19	3.41E-10	f20	8.49E-13	f21	4.50E-15	ne18	3.55E-23
ne19	4.56E-16	ne20	2.28E-01	ne21	3.11E-04	ne22	2.93E-02	ne23	1.83E-07
ne24	1.85E-12	ne25	3.26E-18	na21	1.03E-12	na22	1.33E-07	na23	1.16E-03
na24	8.93E-08	na25	6.21E-11	na26	2.52E-18	mg22	2.51E-17	mg23	3.48E-07
mg24	1.46E-01	mg25	1.86E-02	mg26	1.73E-02	mg27	7.64E-08	mg28	9.24E-11
al24	1.91E-22	al25	1.44E-10	al26	6.77E-06	al27	1.59E-02	al28	1.24E-05
al29	5.21E-08	al30	8.83E-13	si26	1.31E-14	si27	2.64E-07	si28	8.32E-02
si29	1.00E-02	si30	7.71E-03	si31	4.29E-06	si32	1.24E-08	si33	3.51E-16
p28	2.69E-23	p29	3.51E-10	p30	4.90E-05	p31	1.18E-03	p32	1.03E-06
p33	5.80E-07	p34	6.39E-11	p35	6.29E-13	s30	1.45E-14	s31	2.32E-08
s32	2.40E-02	s33	1.20E-04	s34	1.26E-03	s35	4.89E-07	s36	4.65E-07
s37	9.15E-16	s38	7.00E-17	cl32	4.32E-22	cl33	1.80E-11	cl34	3.36E-09
cl35	5.18E-05	cl36	6.63E-07	cl37	8.10E-07	cl38	2.95E-11	cl39	5.73E-13
cl40	8.50E-17	ar34	8.83E-15	ar35	3.69E-09	ar36	4.15E-03	ar37	6.14E-06
ar38	3.72E-04	ar39	2.57E-09	ar40	3.39E-09	ar41	1.20E-12	ar42	2.79E-14
ar43	5.88E-18	ar44	1.05E-19	k36	3.18E-19	k37	6.99E-13	k38	1.91E-07
k39	2.80E-05	k40	8.18E-09	k41	2.65E-09	k42	2.83E-11	k43	1.86E-12
k44	6.51E-14	k45	5.86E-15	k46	5.89E-17	ca38	1.31E-17	ca39	9.21E-10
ca40	3.73E-03	ca41	1.92E-06	ca42	1.04E-05	ca43	1.02E-08	ca44	6.13E-09
ca45	8.25E-12	ca46	9.00E-12	ca47	4.35E-14	ca48	8.56E-16	ca49	8.96E-22
sc40	1.39E-22	sc41	6.17E-15	sc42	1.47E-10	sc43	2.58E-06	sc44	8.99E-10
sc45	3.21E-09	sc46	6.52E-11	sc47	1.37E-11	sc48	3.31E-13	sc49	9.21E-15
sc50	5.53E-19	ti42	2.68E-25	ti43	2.37E-12	ti44	1.70E-04	ti45	7.95E-08
ti46	3.84E-06	ti47	9.86E-08	ti48	3.38E-08	ti49	1.36E-10	ti50	1.39E-10
ti51	3.75E-16	ti52	1.81E-17	v44	2.60E-23	v45	2.06E-13	v46	3.61E-14
v47	7.14E-06	v48	2.65E-08	v49	3.46E-08	v50	3.40E-10	v51	2.54E-09
v52	6.49E-14	v53	9.30E-16	v54	2.58E-20	cr46	1.76E-20	cr47	2.30E-10
cr48	2.15E-04	cr49	4.10E-06	cr50	3.54E-05	cr51	5.19E-07	cr52	5.61E-06
cr53	1.41E-09	cr54	6.23E-11	cr55	1.07E-17	cr56	4.20E-19	mn48	3.26E-23
mn49	2.67E-14	mn50	1.84E-14	mn51	1.13E-05	mn52	3.71E-07	mn53	3.79E-06
mn54	1.50E-08	mn55	5.46E-09	mn56	2.37E-14	mn57	5.33E-17	mn58	9.77E-22
fe51	5.69E-16	fe52	9.32E-04	fe53	8.32E-05	fe54	3.29E-03	fe55	1.25E-05
fe56	4.03E-05	fe57	4.83E-09	fe58	2.84E-10	fe59	1.21E-16	fe60	8.16E-19
fe61	1.81E-25	co53	2.28E-18	co54	7.39E-15	co55	3.03E-04	co56	7.11E-06
co57	2.73E-06	co58	4.76E-09	co59	2.13E-09	co60	3.63E-14	co61	5.09E-16
co62	3.76E-22	co63	2.06E-22	ni55	1.63E-18	ni56	7.39E-02	ni57	2.89E-03
ni58	3.98E-03	ni59	1.11E-05	ni60	5.02E-06	ni61	4.11E-09	ni62	3.95E-09
ni63	9.73E-16	ni64	4.80E-17	ni65	9.06E-24	ni66	1.82E-24	cu57	1.09E-12
cu58	8.27E-08	cu59	9.27E-05	cu60	1.20E-04	cu61	1.12E-05	cu62	3.95E-07
cu63	3.90E-09	cu64	1.45E-14	cu65	6.34E-16	cu66	3.24E-21	cu67	2.10E-22
zn59	1.15E-20	zn60	2.21E-03	zn61	1.29E-04	zn62	9.34E-04	zn63	1.07E-06
zn64	5.50E-08	zn65	1.46E-09	zn66	1.57E-11	zn67	1.17E-14	zn68	1.67E-17
zn69	1.88E-24	zn70	1.58E-25	ga61	3.30E-18	ga62	4.41E-19	ga63	7.10E-07
ga64	1.80E-06	ga65	3.19E-07	ga66	3.17E-08	ga67	6.71E-10	ga68	1.05E-14
ga69	1.02E-15	ga70	2.49E-20	ga71	1.86E-23	ge63	3.95E-23	ge64	1.38E-05
ge65	1.17E-06	ge66	2.11E-05	ge67	8.19E-08	ge68	1.16E-08	ge69	4.89E-12
ge70	1.74E-14	ge71	2.41E-18	ge72	6.00E-21	ge73	1.09E-25	ge74	3.65E-24

TABLE 8B

COMPOSITION OF EJECTA $M = 20\ M_\odot$, ORIGINAL Y_e

	M/M⊙		M/M⊙		M/M⊙		M/M⊙		M/M⊙
d	4.05E-17	t	6.17E-20	he3	2.50E-19	he4	2.10E+00	li6	6.09E-19
li7	5.40E-20	be7	5.56E-22	be9	8.21E-18	be10	1.52E-21	b10	3.24E-17
b11	1.04E-14	b12	6.12E-24	c11	1.25E-17	c12	1.14E-01	c13	4.86E-07
c14	1.00E-08	c15	1.87E-14	n13	8.19E-11	n14	2.71E-03	n15	5.06E-08
n16	5.53E-13	n17	1.38E-18	o14	3.46E-18	o15	1.48E-11	o16	1.48E+00
o17	1.84E-08	o18	8.68E-03	o19	8.07E-10	o20	1.78E-13	f17	5.35E-15
f18	2.37E-08	f19	3.41E-10	f20	8.49E-13	f21	4.50E-15	ne18	3.21E-23
ne19	4.56E-16	ne20	2.28E-01	ne21	3.11E-04	ne22	2.93E-02	ne23	1.83E-07
ne24	1.85E-12	ne25	3.26E-18	na21	1.02E-12	na22	1.33E-07	na23	1.16E-03
na24	8.93E-08	na25	6.21E-11	na26	2.52E-18	mg22	2.30E-17	mg23	3.48E-07
mg24	1.46E-01	mg25	1.86E-02	mg26	1.73E-02	mg27	7.64E-08	mg28	9.24E-11
al24	1.91E-22	al25	1.14E-10	al26	6.77E-06	al27	1.59E-02	al28	1.24E-05
al29	5.21E-08	al30	8.83E-13	si26	8.69E-15	si27	2.64E-07	si28	8.32E-02
si29	1.00E-02	si30	7.71E-03	si31	4.29E-06	si32	1.24E-08	si33	3.51E-16
p28	2.61E-23	p29	2.45E-10	p30	4.90E-05	p31	1.18E-03	p32	1.03E-06
p33	5.80E-07	p34	6.39E-11	p35	6.29E-13	s30	1.08E-14	s31	2.32E-08
s32	2.40E-02	s33	1.20E-04	s34	1.26E-03	s35	4.89E-07	s36	4.65E-07
s37	9.15E-16	s38	7.00E-17	cl32	4.17E-22	cl33	1.20E-11	cl34	3.22E-09
cl35	5.17E-05	cl36	6.64E-07	cl37	8.10E-07	cl38	2.95E-11	cl39	5.73E-13
cl40	8.50E-17	ar34	6.40E-15	ar35	3.12E-09	ar36	4.14E-03	ar37	6.16E-06
ar38	3.73E-04	ar39	2.58E-09	ar40	3.42E-09	ar41	1.20E-12	ar42	2.79E-14
ar43	5.88E-18	ar44	1.05E-19	k36	3.17E-19	k37	5.45E-13	k38	2.01E-07
k39	2.88E-05	k40	8.42E-09	k41	2.79E-09	k42	2.83E-11	k43	1.86E-12
k44	6.51E-14	k45	5.86E-15	k46	5.89E-17	ca38	8.35E-18	ca39	9.51E-10
ca40	3.72E-03	ca41	2.18E-06	ca42	1.10E-05	ca43	1.01E-08	ca44	6.15E-09
ca45	8.25E-12	ca46	9.00E-12	ca47	4.35E-14	ca48	8.56E-16	ca49	8.96E-22
sc40	1.44E-22	sc41	6.23E-15	sc42	3.22E-10	sc43	2.31E-06	sc44	1.70E-09
sc45	4.84E-09	sc46	6.53E-11	sc47	1.37E-11	sc48	3.31E-13	sc49	9.21E-15
sc50	5.53E-19	ti42	2.68E-25	ti43	2.10E-12	ti44	1.53E-04	ti45	1.34E-07
ti46	4.00E-06	ti47	8.74E-08	ti48	3.38E-08	ti49	1.36E-10	ti50	1.39E-10
ti51	3.75E-16	ti52	1.81E-17	v44	2.64E-23	v45	2.03E-13	v46	9.59E-16
v47	4.96E-06	v48	3.13E-08	v49	3.54E-08	v50	3.41E-10	v51	2.54E-09
v52	6.49E-14	v53	9.30E-16	v54	2.58E-20	cr46	1.64E-20	cr47	3.31E-10
cr48	1.99E-04	cr49	4.17E-06	cr50	3.55E-05	cr51	5.20E-07	cr52	5.61E-06
cr53	1.41E-09	cr54	6.23E-11	cr55	1.07E-17	cr56	4.20E-19	mn48	5.03E-23
mn49	2.41E-14	mn50	5.16E-14	mn51	1.17E-05	mn52	3.83E-07	mn53	3.81E-06
mn54	1.50E-08	mn55	5.46E-09	mn56	2.37E-14	mn57	5.33E-17	mn58	9.77E-22
fe51	8.66E-16	fe52	9.14E-04	fe53	8.45E-05	fe54	3.29E-03	fe55	1.25E-05
fe56	4.03E-05	fe57	4.84E-09	fe58	2.84E-10	fe59	1.21E-16	fe60	8.16E-19
fe61	1.81E-25	co53	2.47E-18	co54	1.72E-14	co55	3.03E-04	co56	7.74E-06
co57	3.45E-06	co58	5.15E-09	co59	2.16E-09	co60	3.65E-14	co61	5.09E-16
co62	3.76E-22	co63	2.06E-22	ni55	1.93E-18	ni56	6.78E-02	ni57	3.12E-03
ni58	9.35E-03	ni59	1.58E-05	ni60	4.18E-06	ni61	4.86E-09	ni62	1.35E-08
ni63	7.64E-15	ni64	8.74E-17	ni65	2.13E-23	ni66	1.82E-24	cu57	1.09E-12
cu58	7.08E-08	cu59	1.30E-04	cu60	9.65E-05	cu61	1.23E-05	cu62	1.28E-06
cu63	3.12E-08	cu64	3.85E-13	cu65	9.17E-15	cu66	1.39E-19	cu67	2.20E-22
zn59	1.01E-20	zn60	1.89E-03	zn61	1.42E-04	zn62	2.12E-03	zn63	6.79E-06
zn64	1.67E-07	zn65	2.60E-09	zn66	9.25E-11	zn67	7.35E-14	zn68	2.55E-16
zn69	1.41E-22	zn70	1.58E-25	ga61	3.45E-18	ga62	6.08E-19	ga63	7.74E-07
ga64	1.71E-06	ga65	4.78E-07	ga66	9.36E-08	ga67	3.51E-09	ga68	1.52E-13
ga69	3.84E-14	ga70	1.97E-18	ga71	2.40E-21	ge63	2.96E-23	ge64	1.05E-05
ge65	1.72E-06	ge66	4.80E-05	ge67	3.82E-07	ge68	1.18E-07	ge69	1.09E-10
ge70	1.04E-12	ge71	3.04E-16	ge72	6.07E-19	ge73	6.34E-23	ge74	3.65E-24

TABLE 9

COMPOSITION OF EJECTA $M = 25\ M_\odot$

	M/M$_\odot$		M/M$_\odot$		M/M$_\odot$		M/M$_\odot$		M/M$_\odot$
d	1.22E-25	t	3.62E-19	he3	7.32E-19	he4	1.95E+00	be10	5.76E-24
b10	2.91E-23	b11	5.29E-14	b12	9.02E-25	c11	1.71E-17	c12	1.48E-01
c13	1.03E-08	c14	9.15E-09	n13	4.99E-13	n14	9.53E-04	n15	1.04E-08
n16	2.31E-21	n17	3.54E-23	o14	2.42E-17	o15	2.55E-11	o16	2.99E+00
o17	7.86E-08	o18	6.69E-03	o19	1.80E-16	o20	1.60E-18	f17	6.60E-17
f18	3.50E-10	f19	8.17E-10	f20	6.20E-12	f21	4.36E-13	ne18	3.49E-22
ne19	9.33E-16	ne20	5.94E-01	ne21	3.22E-03	ne22	3.39E-02	ne23	8.37E-10
ne24	2.05E-13	ne25	7.92E-21	na21	1.82E-13	na22	2.56E-07	na23	1.81E-02
na24	2.73E-06	na25	6.64E-09	na26	7.14E-13	mg22	1.35E-16	mg23	1.92E-06
mg24	1.59E-01	mg25	3.92E-02	mg26	3.17E-02	mg27	4.72E-07	mg28	1.56E-09
al24	3.63E-19	al25	6.33E-13	al26	9.73E-06	al27	1.95E-02	al28	3.79E-05
al29	3.38E-07	al30	1.08E-10	si26	1.64E-13	si27	1.98E-06	si28	1.03E-01
si29	6.97E-03	si30	6.81E-03	si31	8.57E-06	si32	4.77E-08	si33	1.38E-14
p27	1.77E-25	p28	1.19E-18	p29	5.59E-11	p30	3.89E-06	p31	8.93E-04
p32	1.71E-06	p33	9.61E-07	p34	3.96E-10	p35	5.59E-12	s29	5.02E-23
s30	1.58E-13	s31	1.50E-07	s32	3.84E-02	s33	2.19E-04	s34	2.77E-03
s35	7.67E-07	s36	7.28E-07	s37	2.81E-15	s38	2.14E-16	cl31	1.10E-25
cl32	6.49E-18	cl33	7.04E-12	cl34	3.38E-08	cl35	6.63E-05	cl36	1.19E-06
cl37	1.56E-06	cl38	5.52E-11	cl39	1.98E-12	cl40	6.14E-16	ar33	3.32E-20
ar34	2.19E-12	ar35	4.33E-08	ar36	6.71E-03	ar37	1.17E-05	ar38	7.24E-04
ar39	5.09E-09	ar40	7.06E-09	ar41	2.66E-12	ar42	1.16E-13	ar43	5.46E-17
ar44	2.68E-18	k35	5.76E-25	k36	8.22E-16	k37	1.14E-12	k38	3.49E-08
k39	3.44E-05	k40	1.68E-08	k41	5.71E-09	k42	6.91E-11	k43	6.75E-12
k44	5.45E-13	k45	1.13E-13	k46	2.88E-15	ca37	4.56E-19	ca38	1.79E-12
ca39	2.36E-07	ca40	6.14E-03	ca41	2.78E-06	ca42	1.77E-05	ca43	1.90E-08
ca44	1.96E-08	ca45	2.98E-11	ca46	3.56E-11	ca47	5.30E-13	ca48	1.70E-14
ca49	5.68E-20	sc40	1.34E-18	sc41	9.42E-15	sc42	2.10E-08	sc43	9.55E-08
sc44	8.27E-10	sc45	6.12E-09	sc46	2.24E-10	sc47	5.26E-11	sc48	2.62E-12
sc49	1.27E-13	sc50	3.01E-17	ti42	1.40E-16	ti43	1.64E-07	ti44	2.11E-05
ti45	8.34E-08	ti46	6.84E-06	ti47	1.22E-07	ti48	8.08E-08	ti49	5.12E-10
ti50	5.90E-10	ti51	9.21E-15	ti52	1.60E-15	v44	8.05E-15	v45	3.04E-12
v46	4.10E-09	v47	2.94E-07	v48	1.75E-08	v49	3.84E-08	v50	7.99E-10
v51	5.84E-09	v52	3.56E-13	v53	5.93E-14	v54	4.56E-18	cr46	2.21E-11
cr47	4.96E-07	cr48	8.97E-05	cr49	5.97E-06	cr50	5.01E-05	cr51	8.95E-07
cr52	9.20E-06	cr53	2.30E-09	cr54	1.19E-10	cr55	1.26E-16	cr56	1.16E-16
mn48	1.05E-13	mn49	5.88E-11	mn50	6.47E-09	mn51	8.94E-06	mn52	2.30E-07
mn53	4.77E-06	mn54	2.40E-08	mn55	8.95E-09	mn56	4.28E-14	mn57	5.01E-15
mn58	1.26E-18	fe50	1.37E-12	fe51	1.16E-07	fe52	1.30E-03	fe53	1.34E-04
fe54	4.81E-03	fe55	2.34E-05	fe56	6.92E-05	fe57	7.79E-09	fe58	4.70E-10
fe59	2.26E-16	fe60	4.17E-16	fe61	1.07E-21	fe62	3.51E-21	co52	3.08E-16
co53	1.77E-12	co54	4.46E-08	co55	4.79E-04	co56	2.46E-06	co57	2.90E-06
co58	7.87E-09	co59	3.76E-09	co60	6.25E-14	co61	6.24E-15	co62	4.47E-19
co63	6.91E-18	ni54	1.18E-14	ni55	5.35E-08	ni56	5.24E-02	ni57	1.15E-03
ni58	1.33E-03	ni59	8.98E-07	ni60	2.54E-06	ni61	6.31E-10	ni62	3.01E-10
ni63	8.82E-16	ni64	5.10E-15	ni65	3.26E-20	ni66	2.58E-18	ni67	8.11E-24
cu57	1.07E-12	cu58	1.26E-07	cu59	2.10E-05	cu60	1.99E-06	cu61	1.13E-07
cu62	8.47E-09	cu63	2.41E-11	cu64	7.93E-16	cu65	5.68E-15	cu66	6.21E-19
cu67	4.64E-17	cu68	8.32E-22	cu69	1.27E-20	zn59	2.13E-11	zn60	6.62E-04
zn61	2.73E-05	zn62	1.70E-04	zn63	6.36E-08	zn64	5.89E-10	zn65	1.21E-12
zn66	1.07E-13	zn67	7.61E-18	zn68	1.88E-16	zn69	5.13E-21	zn70	2.44E-18
zn71	1.40E-23	zn72	1.88E-21	ga61	1.52E-14	ga62	3.37E-09	ga63	8.66E-08
ga64	2.54E-08	ga65	1.92E-09	ga66	4.00E-10	ga67	1.72E-12	ga68	4.61E-17
ga69	2.18E-17	ga70	5.00E-20	ga71	3.65E-18	ga72	3.23E-22	ga73	9.45E-20
ga74	2.50E-23	ge63	1.89E-13	ge64	3.08E-06	ge65	1.40E-07	ge66	2.58E-06
ge67	2.94E-09	ge68	9.29E-10	ge69	7.99E-14	ge70	5.15E-16	ge71	5.85E-20
ge72	4.78E-18	ge73	1.65E-21	ge74	3.22E-19	ge75	3.18E-23	ge76	2.94E-20
ge77	1.32E-24	ge78	5.90E-23						

that ^{52}Fe and ^{48}Cr have a significant contribution from incomplete Si burning. An educated guess for the change should be based on the abundances in complete Si burning in the inner mass zones and the change of the mass cut reflected by the scaling of ^{56}Ni. Tables 10, 11, 12A–B, and 13 correspond to Tables 6A, 7, 8A–8B, and 9 after decay of radioactive species. A change of the amount of the ^{56}Ni ejecta decaying to ^{56}Fe, as discussed above, should be carried over through the decay.

For major elements, the dependence of the ejecta from the progenitor mass was already summarized in Table 3. The content of Table 3 indicates an interesting behavior. While the heavier intermediate-mass nuclei originate only from explosive O and Si burning, which contribute similar amounts for all progenitor masses (see also Table 1), the lighter elements, C through Mg, have dominant or essential contributions from hydrostatic burning (C/Ne core) or explosive Ne burning. For both latter cases, we see a tremendous mass dependence in Table 1 and a strong reduction of the involved mass zones for less massive starts.

4. OBSERVATIONAL CONSTRAINTS

4.1. *Stellar Models*

There exist a number of quantitative comparisons for SN 1987A (a 20 $M_\odot$ star during its main-sequence evolution)

TABLE 10

COMPOSITION AFTER DECAY $M = 13\ M_\odot$

	M/M$_\odot$		M/M$_\odot$		M/M$_\odot$		M/M$_\odot$
d	2.62E-27	he3	1.01E-18	he4	1.46E+00	li7	1.67E-25
b10	4.00E-23	b11	4.26E-14	c12	5.94E-02	c13	6.23E-09
n14	6.09E-03	n15	2.65E-08	o16	2.05E-01	o17	6.44E-08
o18	1.01E-02	f19	9.40E-10	ne20	2.49E-02	ne21	2.31E-04
ne22	2.92E-03	na23	8.04E-04	mg24	9.63E-03	mg25	1.50E-03
mg26	1.02E-03	al27	1.08E-03	si28	4.77E-02	si29	6.52E-04
si30	1.41E-03	p31	2.38E-04	s32	2.36E-02	s33	1.05E-04
s34	1.36E-03	s36	3.00E-07	cl35	3.82E-05	cl37	9.05E-06
ar36	4.45E-03	ar38	4.90E-04	ar40	4.80E-09	k39	2.71E-05
k41	2.30E-06	ca40	4.25E-03	ca42	1.29E-05	ca43	9.26E-07
ca44	5.56E-05	ca46	1.59E-10	ca48	9.77E-14	sc45	8.06E-08
ti46	4.89E-06	ti47	3.64E-06	ti48	1.36E-04	ti49	5.52E-06
ti50	1.15E-10	v50	5.05E-10	v51	1.17E-05	cr50	4.50E-05
cr52	1.42E-03	cr53	1.40E-04	cr54	2.29E-08	mn55	5.69E-04
fe54	4.32E-03	fe56	1.53E-01	fe57	4.59E-03	fe58	8.35E-09
co59	1.26E-04	ni58	6.07E-03	ni60	3.15E-03	ni61	1.39E-04
ni62	9.29E-04	ni64	1.18E-15	cu63	7.90E-07	cu65	6.80E-07
zn64	1.42E-05	zn66	1.38E-05	zn67	1.47E-08	zn68	4.89E-09
zn70	1.07E-22	ga69	3.64E-13	ga71	7.18E-20	ge70	2.97E-15
ge72	6.17E-23	ge73	5.72E-24	ge74	2.93E-25	ge76	1.87E-25

between nucleosynthesis predictions and observations (see, e.g., Table 2 in Danziger et al. 1990, § IVb in Thielemann et al. 1990, Bouchet, Danziger, & Lucy 1991, or McCray 1993), which show reasonable agreement for C, O, Si, Cl, Ar, Co, and Ni (or Fe) between observation and theory. We want to concentrate here on a crucial aspect, the O abundance.

The amount of ^{16}O is closely linked to the "effective" $^{12}C(\alpha, \gamma)^{16}O$ rate during core He burning. This effective rate is determined by three factors: (1) the actual nuclear rate, (2) the amount of overshooting, mixing fresh He fuel into the core at late phases of He burning, when the temperatures are relatively high and favor alpha captures on ^{12}C, and (3) the stellar mass or He core size, which determines the central temperature during He burning.

The nuclear rate is still not fully determined. We performed these investigations with the rate by Caughlan et al. (1985), which is one choice within the uncertainties left by experiments (see, e.g., Filippone et al. 1989; Humblet, Filippone, & Koonin 1991; Barker & Kajino 1991; Buchmann et al. 1993; Zhao et al. 1993a, b; Azuma et al. 1994; Mohr et

TABLE 11

COMPOSITION AFTER DECAY $M = 15\ M_\odot$

	M/M$_\odot$		M/M$_\odot$		M/M$_\odot$		M/M$_\odot$
d	3.03E-26	he3	8.40E-20	he4	1.83E+00	b10	6.47E-24
b11	2.03E-15	c12	8.33E-02	c13	4.98E-10	n14	5.37E-03
n15	1.58E-10	o16	4.23E-01	o17	5.08E-09	o18	1.35E-02
f19	2.67E-11	ne20	2.83E-02	ne21	4.53E-05	ne22	1.26E-02
na23	2.09E-04	mg24	4.20E-02	mg25	3.46E-03	mg26	2.52E-03
al27	5.56E-03	si28	6.52E-02	si29	4.40E-03	si30	4.91E-03
p31	8.67E-04	s32	2.16E-02	s33	9.31E-05	s34	1.09E-03
s36	5.38E-07	cl35	5.48E-05	cl37	5.62E-06	ar36	3.49E-03
ar38	3.26E-04	ar40	4.89E-09	k39	1.71E-05	k41	1.25E-06
ca40	3.03E-03	ca42	6.98E-06	ca43	1.21E-06	ca44	7.19E-05
ca46	5.45E-11	ca48	6.71E-16	sc45	4.66E-08	ti46	2.72E-06
ti47	4.67E-06	ti48	1.27E-04	ti49	4.15E-06	ti50	4.59E-10
v50	3.51E-10	v51	1.01E-05	cr50	3.85E-05	cr52	8.24E-04
cr53	8.92E-05	cr54	1.55E-08	mn55	3.39E-04	fe54	3.51E-03
fe56	1.30E-01	fe57	4.64E-03	fe58	3.62E-09	co59	1.36E-04
ni58	6.64E-03	ni60	3.13E-03	ni61	1.46E-04	ni62	1.00E-03
ni64	1.73E-15	cu63	9.56E-07	cu65	7.69E-07	zn64	1.41E-05
zn66	1.47E-05	zn67	1.94E-08	zn68	6.35E-09	zn70	3.19E-21
ga69	6.47E-13	ga71	2.05E-19	ge70	5.13E-15	ge72	5.57E-20
ge73	7.68E-23	ge74	1.12E-21	ge76	4.37E-24		9.28E-16

TABLE 12A

COMPOSITION AFTER DECAY $M = 20\ M_\odot$

	M/M$_\odot$		M/M$_\odot$		M/M$_\odot$		M/M$_\odot$
d	4.05E-17	he3	3.11E-19	he4	2.10E+00	li6	6.09E-19
li7	5.46E-20	be9	8.21E-18	b10	3.24E-17	b11	1.04E-14
c12	1.14E-01	c13	4.86E-07	n14	2.71E-03	n15	5.06E-08
o16	1.48E+00	o17	1.84E-08	o18	8.68E-03	f19	1.15E-09
ne20	2.28E-01	ne21	3.11E-04	ne22	2.93E-02	na23	1.16E-03
mg24	1.46E-01	mg25	1.86E-02	mg26	1.73E-02	al27	1.59E-02
si28	8.33E-02	si29	1.00E-02	si30	7.76E-03	p31	1.18E-03
s32	2.40E-02	s33	1.21E-04	s34	1.26E-03	s36	4.78E-07
cl35	5.23E-05	cl37	6.95E-06	ar36	4.15E-03	ar38	3.72E-04
ar40	4.29E-09	k39	2.80E-05	k41	1.92E-06	ca40	3.73E-03
ca42	1.04E-05	ca43	2.59E-06	ca44	1.70E-04	ca46	7.42E-11
ca48	8.56E-16	sc45	8.27E-08	ti46	3.84E-06	ti47	7.24E-06
ti48	2.15E-04	ti49	4.13E-06	ti50	1.39E-10	v50	3.40E-10
v51	1.18E-05	cr50	3.54E-05	cr52	9.38E-04	cr53	8.70E-05
cr54	1.51E-08	mn55	3.16E-04	fe54	3.29E-03	fe56	7.40E-02
fe57	2.89E-03	fe58	5.04E-09	co59	1.04E-04	ni58	3.98E-03
ni60	2.34E-03	ni61	1.40E-04	ni62	9.34E-04	ni64	1.80E-14
cu63	1.79E-06	cu65	1.49E-06	zn64	1.57E-05	zn66	2.11E-05
zn67	8.25E-08	zn68	1.16E-08	zn70	1.58E-25	ga69	4.89E-12
ga71	2.41E-18	ge70	1.74E-14	ge72	6.00E-21	ge73	1.09E-25
ge74	3.65E-24						

TABLE 12B

COMPOSITION AFTER DECAY $M = 20\ M_\odot$, ORIGINAL Y_e

	M/M$_\odot$		M/M$_\odot$		M/M$_\odot$		M/M$_\odot$
d	4.05E-17	he3	3.11E-19	he4	2.10E+00	li6	6.09E-19
li7	5.46E-20	be9	8.21E-18	b10	3.24E-17	b11	1.04E-14
c12	1.14E-01	c13	4.86E-07	n14	2.71E-03	n15	5.06E-08
o16	1.48E+00	o17	1.84E-08	o18	8.68E-03	f19	1.15E-09
ne20	2.28E-01	ne21	3.11E-04	ne22	2.93E-02	na23	1.16E-03
mg24	1.46E-01	mg25	1.86E-02	mg26	1.73E-02	al27	1.59E-02
si28	8.33E-02	si29	1.00E-02	si30	7.76E-03	p31	1.18E-03
s32	2.40E-02	s33	1.21E-04	s34	1.26E-03	s36	4.78E-07
cl35	5.22E-05	cl37	6.97E-06	ar36	4.14E-03	ar38	3.73E-04
ar40	4.34E-09	k39	2.88E-05	k41	2.18E-06	ca40	3.72E-03
ca42	1.10E-05	ca43	2.32E-06	ca44	1.53E-04	ca46	7.43E-11
ca48	8.56E-16	sc45	1.39E-07	ti46	4.00E-06	ti47	5.04E-06
ti48	1.99E-04	ti49	4.20E-06	ti50	1.39E-10	v50	3.41E-10
v51	1.22E-05	cr50	3.55E-05	cr52	9.20E-04	cr53	8.83E-05
cr54	1.51E-08	mn55	3.15E-04	fe54	3.29E-03	fe56	6.78E-02
fe57	3.13E-03	fe58	5.43E-09	co59	1.46E-04	ni58	9.35E-03
ni60	1.99E-03	ni61	1.54E-04	ni62	2.12E-03	ni64	4.77E-13
cu63	7.60E-06	cu65	2.20E-06	zn64	1.24E-05	zn66	4.80E-05
zn67	3.86E-07	zn68	1.18E-07	zn70	1.58E-25	ga69	1.09E-10
ga71	3.04E-16	ge70	1.04E-12	ge72	6.07E-19	ge73	6.34E-23
ge74	3.65E-24						

TABLE 13

COMPOSITION AFTER DECAY $M = 25\ M_\odot$

	M/M$_\odot$		M/M$_\odot$		M/M$_\odot$		M/M$_\odot$
d	1.22E-25	he3	1.09E-18	he4	1.95E+00	b10	3.48E-23
b11	5.29E-14	c12	1.48E-01	c13	1.03E-08	n14	9.53E-04
n15	1.04E-08	o16	2.99E+00	o17	7.86E-08	o18	6.69E-03
f19	8.17E-10	ne20	5.94E-01	ne21	3.22E-03	ne22	3.39E-02
na23	1.81E-02	mg24	1.59E-01	mg25	3.92E-02	mg26	3.17E-02
al27	1.95E-02	si28	1.03E-01	si29	6.97E-03	si30	6.81E-03
p31	9.02E-04	s32	3.84E-02	s33	2.20E-04	s34	2.77E-03
s36	7.51E-07	cl35	6.72E-05	cl37	1.32E-05	ar36	6.71E-03
ar38	7.24E-04	ar40	8.91E-09	k39	3.47E-05	k41	2.79E-06
ca40	6.14E-03	ca42	1.77E-05	ca43	2.78E-07	ca44	2.11E-05
ca46	2.60E-10	ca48	1.70E-14	sc45	8.96E-08	ti46	6.84E-06
ti47	9.11E-07	ti48	8.98E-05	ti49	6.01E-06	ti50	5.90E-10
v50	7.99E-10	v51	9.96E-06	cr50	5.01E-05	cr52	1.31E-03
cr53	1.39E-04	cr54	2.41E-08	mn55	5.02E-04	fe54	4.81E-03
fe56	5.24E-02	fe57	1.16E-03	fe58	8.34E-09	co59	2.19E-05
ni58	1.33E-03	ni60	6.67E-04	ni61	2.74E-05	ni62	1.70E-04
ni64	6.08E-15	cu63	1.50E-07	cu65	1.41E-07	zn64	3.10E-06
zn66	2.58E-06	zn67	2.94E-09	zn68	9.29E-10	zn70	2.44E-18
ga69	8.00E-14	ga71	3.70E-18	ge70	5.15E-16	ge72	4.78E-18
ge73	9.62E-20	ge74	3.22E-19	ge75	3.18E-23	ge76	2.94E-20
ge77	1.32E-24	ge78	5.90E-23				

al. 1995). The rate is based on an astrophysical S factor of $S_{tot}(0.3\ \mathrm{MeV}) = 0.24$ MeV barn, which is within the error bars of the evaluation of the Münster data (Redder et al. 1987) and the Caltech data (Kremer et al. 1988) undertaken by Barker & Kahino (1991). The resonances of interest are $J^{\pi} = 1^-$ and 2^+ states, which emit electric dipole (E1) and quadrupole (E2) radiation when decaying to the O^+ ground state of ^{16}O. The S factor quoted above is composed of an E1 component in the range 0.08–0.40 and an E2 component of 0.06–0.19 MeV barn (Barker & Kajino 1991). Their result was obtained from best fits to the then available data on alpha capture of ^{12}C, $^{12}C + \alpha$ elastic scattering phase shifts, and the delayed alpha spectrum from ^{16}N decay.

An independent analysis of the data by Humblet et al. (1991) resulted in different error ranges [$S_{E1}(0.3) =$ 0.027–0.063 MeV barn and $S_{E2} = 0.002$–0.031 MeV barn]. More recent experiments by Quillet et al. (1992) came to the surprising result $S_{E1} = 0.0$–0.007 MeV barn and $S_{E2} =$ 0.033–0.047 Mev barn, but are contradicted by the two most recent results of a Triumf and a Yale collaboration (Buchmann et al. 1993; Zhao et al. 1993a, b; Azuma et al. 1994), also based on the beta-delayed alpha emission of ^{16}N. While the quoted results still differ somewhat, $S_{E1} =$ 0.044–0.070 MeV barn from a T-matrix analysis (Buchmann et al.) and 0.095 ± 0.006 MeV barn from an R-matrix analysis (Zhao et al.), a subsequent R-matrix analysis of both experiments yields a value close to 0.080 MeV barn. Unfortunately, the final result for the E2 component is still open. With an expected contribution of the same size as the E1 component (0.080 MeV barn) but uncertain by roughly a factor of 2, we we expect a total S factor at 300 keV of roughly 0.120–0.240 meV barn, which corresponds to the Caughlan & Fowler (1988) rate multiplied by a factor of 1.3–2.4 and includes the value of the Caughlan et al. (1985) rate. As the effect on the astrophysical outcome is dramatic, this issue still requires a final solution. A set of stellar models employing a variation of the $^{12}C(\alpha, \gamma)$ rate will appear in Hashimoto et al. (1995).

As the rate by Caughlan et al. (1985) seems to be close to the barely permitted upper limit, it is crucial to check the observations for individual stellar models, in order to normalize the O production correctly. The model calculations for a 20 $M_{\odot}$ star predict 1.48 $M_{\odot}$ of ejected ^{16}O. This is within the early observational constraints of 0.3–3.0 $M_{\odot}$ (see Table 2 in Danziger et al. 1990) but somewhat unsatisfying. The improved analysis of observations for SN 1987A by Spyromilio & Pinto (1991) helped to put tighter constraints on the precollapse models by increasing the lower limit to 0.7 $M_{\odot}$. Major improvements were possible by modeling of the late nebular spectra (Fransson & Kozma 1993). Fransson, Houck, & Kozma (1995) found a value of about 1.5 $M_{\odot}$. Chugai (1994) determined 1.2–1.5 $M_{\odot}$. Earlier, Li & McCray (1992) noted that they found good agreement with observational spectra when making use of 1.5 $M_{\odot}$. Our value lies well in the remaining uncertainty range, which seems not to ask for a smaller $^{12}C(\alpha, \gamma)^{16}O$ rate than Caughlan et al. (1985). A total S factor of 0.150 MeV barn would reduce the ^{16}O mass, within our treatment of convection, below 1 $M_{\odot}$, a value which seems now excluded. It should, however, be clear that these observations test only the combined effect of nuclear rate and convection treatment (here Schwarzschild without overshooting; see also Langer & Henkel 1995). Similar results were found by Werner et al. (1995) when analyzing spectra of young white dwarfs with models of d'Antonia & Mazzitelli (1992).

The first results from O determinations for SN 1993J are also available now. Houck & Fransson (1996) find a value of ≈ 0.4 $M_{\odot}$. Our prediction of 0.423 $M_{\odot}$ for a 15 $M_{\odot}$ main-sequence star agrees fairly well; SN 1993J was determined to be a 14 ± 1 $M_{\odot}$ star (see discussion in §§ 1 and 2). This leads to the conclusion that the Caughlan et al. (1985) rate, used in conjunction with the Schwarzschild criterion for convection and no overshooting, gives an excellent agreement with observations for individual supernovae. This is the best possible check and is preferable over methods which make use of integrals over stellar populations.

Recently other diagnostics have become available for abundance determinations in supernova remnants. In that case, the progenitor mass is not known, but the relative abundance ratios between different elements can be tested for consistency with abundance predictions for a variety of progenitor masses. Hughes & Singh (1994) made use of X-ray spectra of the supernova remnant G292.0+1.8 and found remarkable agreement for all element ratios from O through Ar with our 25 $M_{\odot}$ calculations (15% rms deviation). This tests implicitly the $^{12}C(\alpha, \gamma)^{16}O$ rate, as it is also reflected in the ratios between C-burning products like Ne and Mg and explosive O-burning products like Ar and S. Comparisons with model predictions, which made use of smaller $^{12}C(\alpha, \gamma)^{16}O$ rates, did not pass that consistency check. UV and optical observations of supernova remnant N132D by Blair, Raymond, & Long (1994) give very good agreement with our element predictions for a 20 $M_{\odot}$ star, with slight deviations for Mg. Thus, we have direct observations of supernovae and supernova remnants ranging from 15 over 20 to 25 $M_{\odot}$, which agree well with our model predictions and indicate that their application for other purposes should be quite reliable.

4.2. Y_e at the Mass Cut and Clues for the Explosion Mechanism

The formation of the nuclei $^{58,61,62}Ni$, which are produced in form of the neutron-rich species ^{58}Ni and $^{61,62}Zn$, is strongly dependent on Y_e and therefore varies with the position of the mass cut between ejected matter and the remaining neutron star (see the discussion in Thielemann et al. 1990 and Kumugai et al. 1991, 1993). Especially for the Ni abundances, the position of the mass cut is crucial. The $^{57}Ni/^{56}Ni$ ratio is correlated with the abundances of stable Ni isotopes, predominantly ^{58}Ni, i.e., with $^{58}Ni/^{56}Ni$. Light-curve observations of SN 1987A (Elias et al. 1991; Bouchet et al. 1991) could be interpreted with a high 57/56 ratio of 4 times solar, but this would also require too large stable Ni abundances not substantiated from observations (Witteborn et al. 1989; Wooden et al. 1993). In order to meet the stable Ni constraints of $3–5 \times 10^{-3}$ $M_{\odot}$ (Danziger et al. 1990; Witteborn et al. 1989; Wooden et al. 1993), only an upper limit of 1.4–1.7 times solar is permitted for the 57/56 ratio (see Tables 8A–8B and 12A–12B). This also agrees well with the observations by Varani et al. (1990) and γ-ray line observations by *GRO* (Kurfess et al. 1992; Clayton et al. 1992). The apparent discrepancy was solved by correct light-curve and spectra modeling with a nonequilibrium treatment of the involved ionization stages at late times (Fransson et al. 1994). This gives a consistent picture for observations of stable Ni, light-curve observations

which are sensitive to ^{56}Co and ^{57}Co decay, and the γ-ray lines emitted from both decays, leading to limits on the abundance ratio of the end products ^{57}Fe/^{56}Fe of 1.4–1.7 times solar.

This corresponds to a Y_e at the mass cut of 0.497 within the little niche in Figure 2*c*. A mass cut at deeper layers, at which Y_e decreases to 0.494, would imply 57/56 ratios larger than 2.5 times solar. A mass cut further out, implying a Y_e of 0.4989, results in a 57/56 ratio of the order of 1 times solar. This means that in order to meet the Y_e constraint with an ejection of 0.075 $M_\odot$ of ^{56}Ni, we have a required delay time of 0.3–0.5 s. Keeping all uncertainties of the model in mind, this can be taken as a strong support that SN 1987A did not explode via a prompt explosion and did not have to wait either for a delayed explosion with a long delay time $t_{de} >$ 0.5 s. The latter would correspond more to a pure neutrino diffusion case, while this result supports the current understanding that entropy gradients drive the convective turnover and cause a faster neutrino transport. The multidimensional calculations by Janka & Müller (1995), Burrows et al. (1995), and Herant et al. (1994) predict delay times of $\approx$0.3 s, in agreement with this finding.

Unfortunately, we do not have yet similar observational and computational results for other supernovae. This would be a strong test for the explosion mechanism as a function of progenitor mass. It is feasible that progenitors exist, where the entropy gradients do not cause strong Rayleigh-Taylor instabilities. Wilson & Mayle (1988) showed clearly that such instabilities can depend on the equation of state used; they would accordingly also depend on the progenitor structure. Therefore, it is important to explore the whole progenitor mass range with multidimensional explosion calculations in order to find out what self-consistent calculations of Y_e would predict for the inner ejecta.

4.3. *Averaged Type II Supernovae Abundance Yields*

Galactic chemical evolution calculations take into account the continuous enrichment of the interstellar medium by SNe I and SNe II, stellar winds (planetary nebulae), etc. In the very early evolution of the Galaxy, only the most massive stars can contribute because of their short lifetime. At time t, only those stars with $\tau_{MS}(M) < t$ can be considered (using the main-sequence lifetime as an approximate measure for the lifetime until the onset of a supernova event in massive stars). If we have varying nucleosynthesis yields with stellar mass, this will lead to varying abundance ratios [x/Fe] in the ISM as a function of time or metallicity [Fe/H] = $\log_{10}$ [(Fe/H)/(Fe/H)$_\odot$], which can, also be taken as a time indicator.

Matteucci (1987), Matteucci & Francois (1989), Mathews, Bazan, & Cowan (1992), and Matteucci et al. (1993) find that, for a typical star formation rate in the solar neighborhood, 30 $M_\odot$ stars will contribute for the first time at [Fe/H] ≈ -3.9, 12 $M_\odot$ stars at -3, and the least massive SNe II somewhere between -3 and -2. Intermediate-mass stars will enrich the interstellar medium for [Fe/H] ≥ -2 via planetary nebular ejection. SNe Ia, which come from binary systems of intermediate-mass stars, are further delayed in time and appear at [Fe/H] ≈ -1. The elements listed in Table 14 can only derive from supernovae (with the exception of C) and therefore can be contributed solely to SNe II for [Fe/H] < -1. In the range $-2.5 \leq$ [Fe/H] ≤ -1, we will expect averaged values for [x/Fe], because SNe II of the whole progenitor mass range contribute. Only below -3 do we expect deviations attributable to the selection effects, singling out more and more massive SNe II with decreasing [Fe/H], which could evolve fast enough to undergo SN II events already at such low metallicities. Therefore, it is not surprising that observations show a constant [x/Fe], x being O, Mg, Si, S, Ca, Ti, Cr, Ni between -2.5 and -1. The integrated yields of SNe II should therefore result in an abundance pattern as found in low-metallicity stars. The latter are taken from the reviews by Gehren (1988), Wheeler, Sneden, & Truran (1989), Lambert (1989), and Pagel (1991), and original papers by "H&G (1988)" (Hartmann & Gehren 1988), "M (1989)" Magain (1989), "M (1990)" (Zhao & Magain 1990), "G & S (1991)" (Gratton & Sneden 1991), and "N (1994)" (Nissen et al. 1994). Except for earlier references mentioned in the cited reviews, we also made use of specific additional observations, all of which are in the column "other sources." These are C/O observations by Abia et al. (1992), which led to the listed range for [C/Fe], and [O/Ar] and [Ne/Ar] observations by Peimbert (1992) as a function of [Ar/H] for very low-metallicity planetary nebulae. These elements are not produced in the planetary nebulae themselves; one sees merely the ratios in the low-metallicity interstellar matter out of which the PN progenitors formed. These observations led to the [Ne/Fe] and [Ar/Fe] ranges which are quoted in the last column. When no error bars are given in Table 14, we assume a typical error of 0.1 dex.

In a first attempt, we have tried a crude method to test whether these considerations are consistent with the results

TABLE 14

ABUNDANCES IN LOW-METALLICITY STARS [x/Fe] FOR [Fe/H] < -1

Element	H&G (1988)	M (1989,1990)	G& S (1991)	N (1994)	other sources
C					-0.34-0.04
O				0.48±0.16	0.5
Ne					0.35-0.85
Mg	0.41	0.47		0.41±0.07	0.4
Si			0.30		0.4
S					0.5
Ar					0.26-0.56
Ca	0.36	0.44	0.29	0.35±0.05	
Sc			-0.03		
Ti	0.14	0.42	0.28	0.27±0.06	
V			-0.03		
Cr			0.04	-0.11±0.07	
Mn			-0.31		
Co			0.12		
Ni			-0.04		
Cu			-0.57		
Zn			0.04		

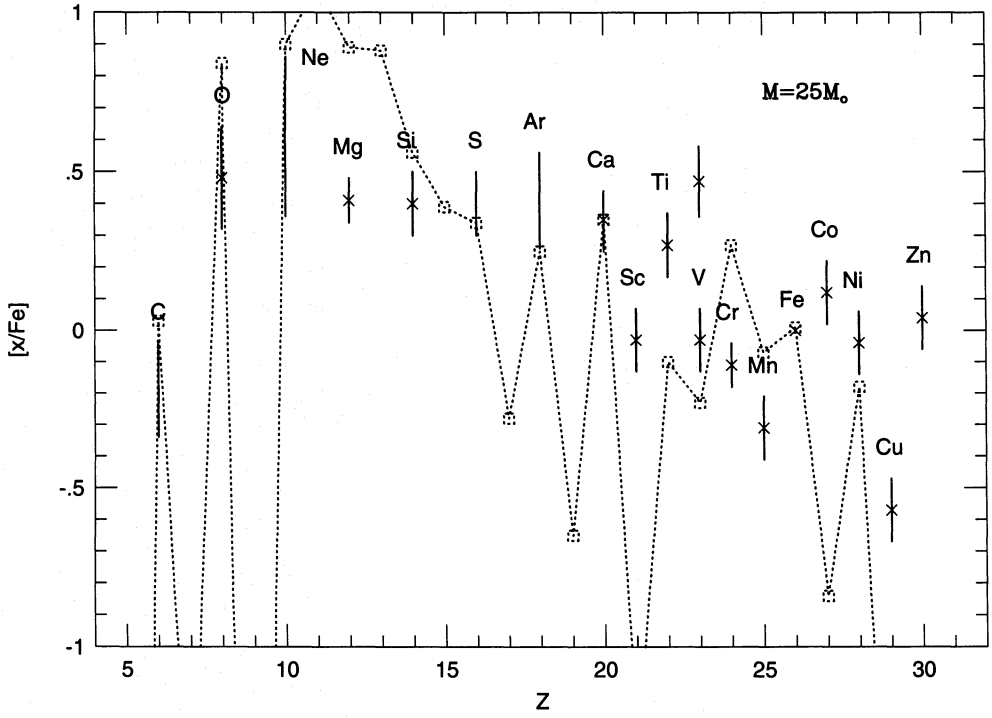

FIG. 5a

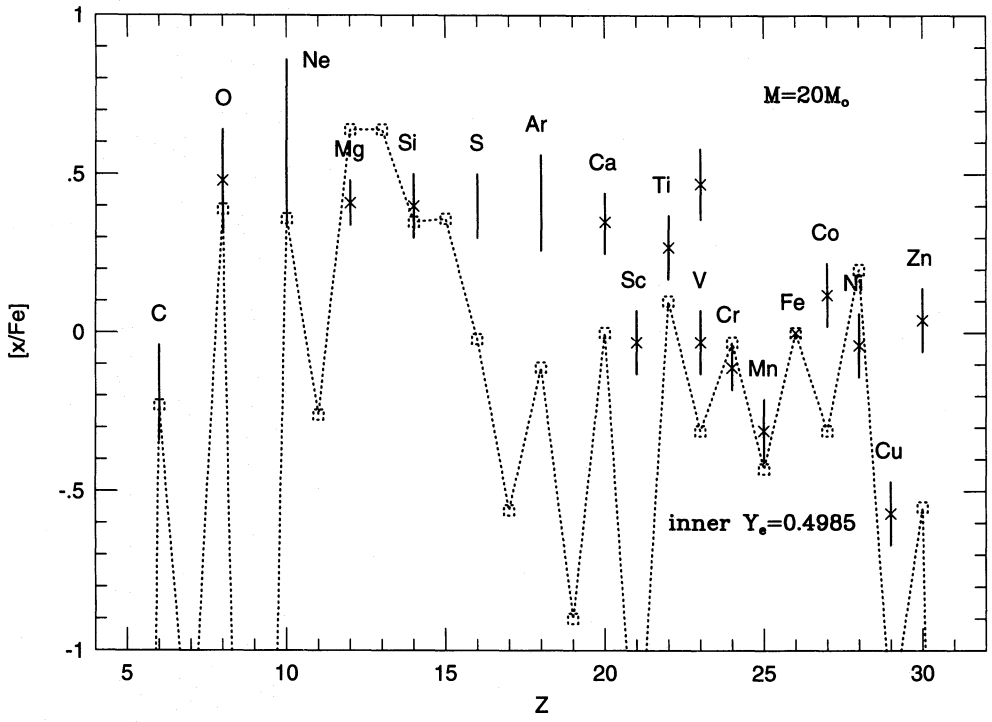

FIG. 5b

FIG. 5.—(*a–h*) A comparison of the results of 13, 15, 20, and 25 $M_\odot$ stars with observations in low-metallicity stars, which represent the average Type II supernovae yields, integrated over an IMF; $[x/Fe] = \log_{10}[(x/Fe)/(x/Fe)_\odot]$ ratios for the different elements characterized by charge number Z are compared to the observations from Table 14 (observations are shown as error bars, and the predicted compositions are displayed as dashed lines). We notice in (*a*) that the 25 $M_\odot$ star overproduces all the elements originating from hydrostatic and explosive Ne/C burning, as expected. The products of explosive O burning are well reproduced, as well as the major products of the Fe group, Fe and Ni. Cu and Zn are strongly underproduced but have different origins (see text). In general, all odd-Z elements of the Fe group are underproduced. In (*b*) the results of the 20 $M_\odot$ star and that this feature of the Fe group abundances depends strongly on Y_e are shown. In general, we see an improvement for $Y_e = 0.4985$. Otherwise, one recognizes a strong decline of the hydrostatic products, expected from the stellar models and a slight decline of explosive products (whose absolute numbers should be relatively constant), as the ratio [x/Fe] is plotted and our choice of Fe ejecta increases with decreasing progenitor mass. This trend continues with progenitor mass through Figures (*c–h*). The major lesson we learn from these figures is that a further decrease of Y_e below 0.4985 leads to a continued increase of odd-Z elements, which is, however, accompanied by a strong increase of the Ni abundance. In an alpha-rich freezeout, the neutron-rich ^{54}Fe is processed to ^{58}Ni and ^{62}Zn (decaying to stable ^{62}Ni). It is obvious that such a composition with huge Ni overabundances cannot play a major role in Type II supernova ejecta. An increase in entropy between (*f*) and (*h*) cannot cure this behavior, but the situation actually worsens. The supernova mechanism must find a way via delay times or multidimensional effects to avoid the ejection of such matter.

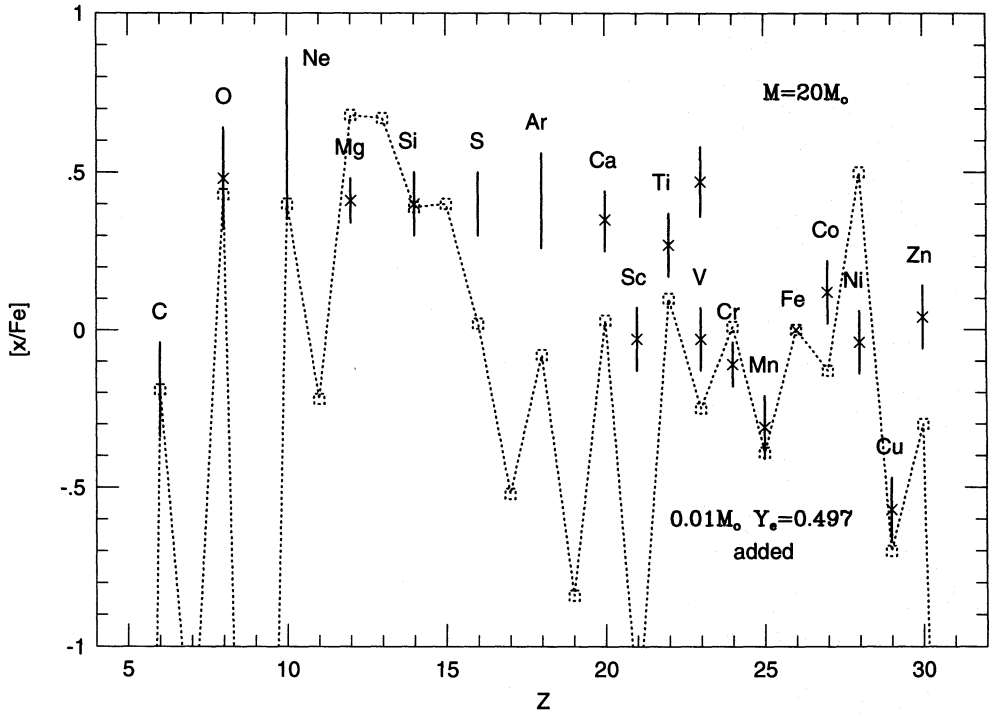

FIG. 5c

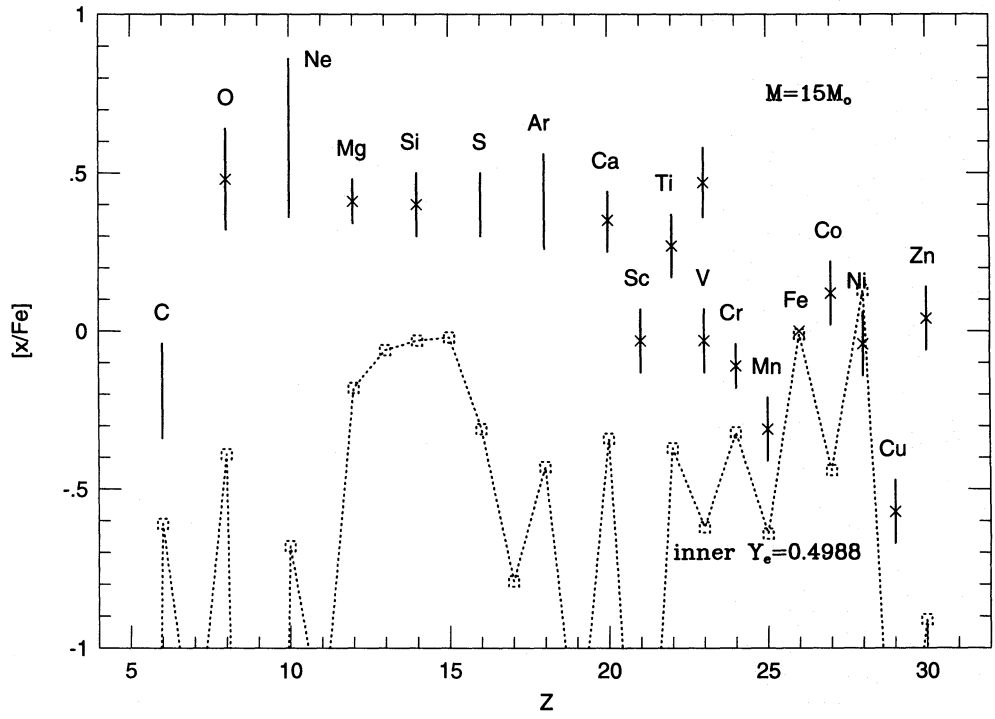

FIG. 5d

from our explosion calculations. We compare the results of our calculations for a grid of 13, 15, 20, and 25 $M_\odot$ stars with these observations. The resulting [x/Fe] ratios are plotted in Figures 5*a*–5*h* and compared to the [x/Fe] values from Table 14. The error bars partially missing in Table 14 have been indicated in the figures. The figures also contain two entries for V, one from V I lines and one from V II lines, but remain very uncertain. From the comparison with the results, it seems that the V I value is preferable.

We want to start the discussion not in order of the mass sequence but in reverse order, as the 25 $M_\odot$ star does not have any Y_e uncertainties for the composition of the inner ejecta. We also have to keep in mind that the abundance pattern observed in low-metalliciy stars does not have to be fitted well by each individual supernova, but that it only represents the integral over all SN II yields. We notice first in Figure 5*a* that the 25 $M_\odot$ star overproduces all the elements originating from hydrostatic and explosive Ne/C burning, as expected from Tables 1 and 3. C, O, Ne, and Mg are overproduced by typically 0.2–0.3 dex. Si, being only

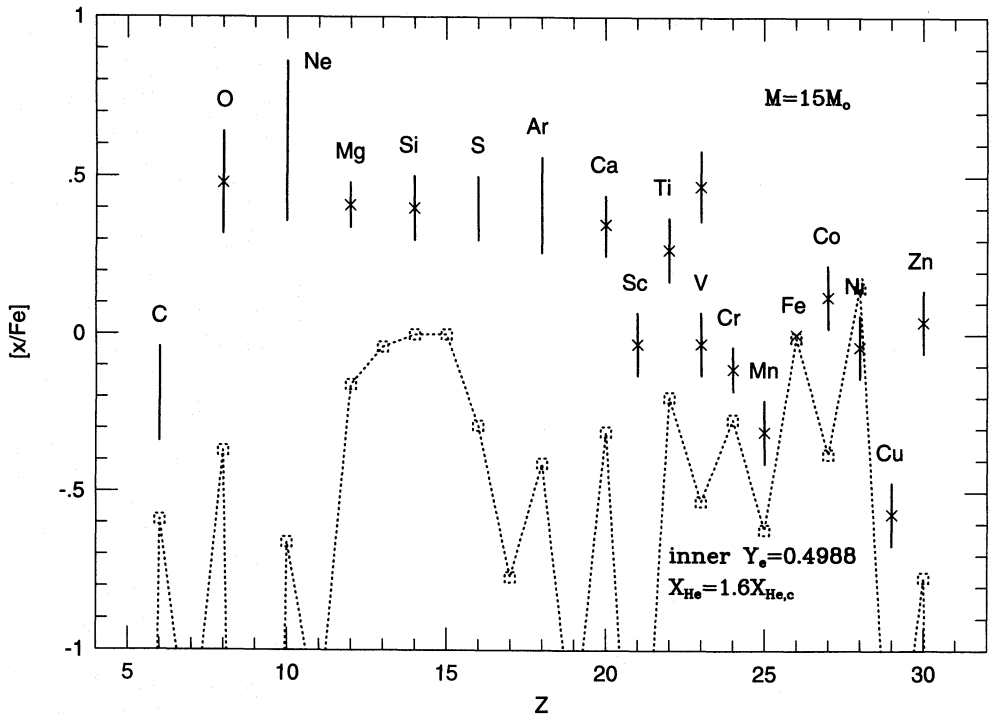

FIG. 5*e*

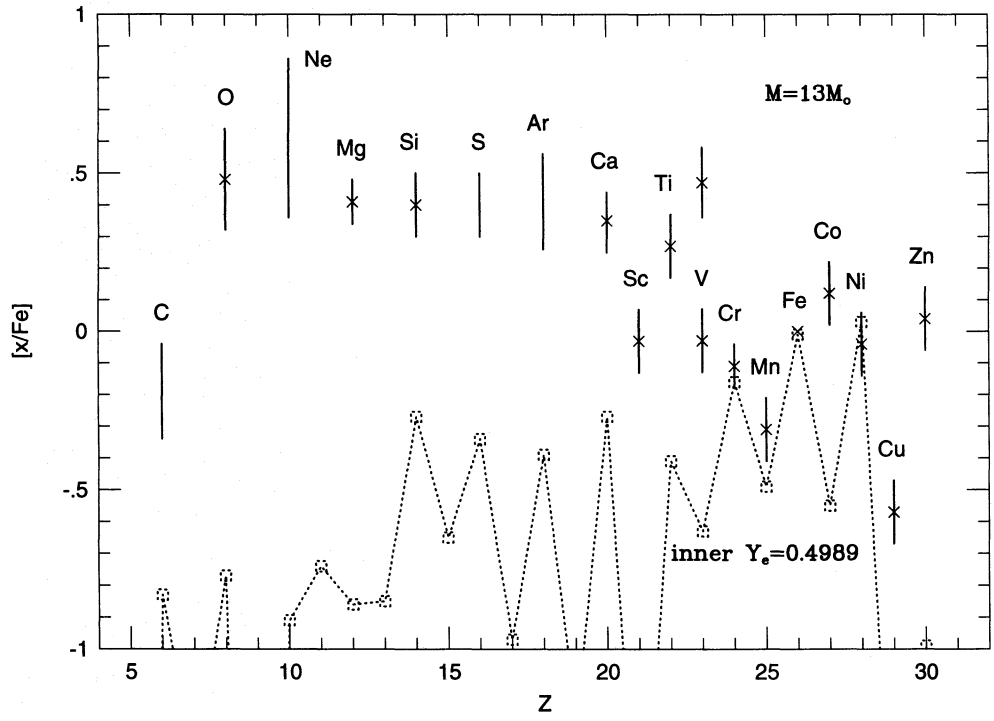

FIG. 5*f*

partially of that origin, features an overproduction of 0.1–0.2 dex. The products of explosive O burning, S, Ar, and Ca, are well reproduced within the error bars. The major products of the Fe group, Fe and Ni, are also well reproduced. Cu and Zn are strongly underproduced. We know that they have an *s*-process and maybe partially SN Ia origin (Matteucci et al. 1993), and we should not expect a strong contribution from SNe II (the weak *s*-process contribution from the hydrostatic precollapse evolution is not included in Fig. 5*a* or any other figure of this series). The choice of a relatively small amount of ^{56}Ni ejecta (0.05 $M_\odot$) also reduces the number of alpha nuclei resulting from the alpha-rich freezeout in the inner mass zones, most noticeably seen in the low Ti abundance (^{48}Ti from ^{48}Cr decay). Owing to a highly energetic explosion, necessary to overcome the gravitational potential of the massive envelope, large amounts of incomplete Si-burning products are produced. These are, among others, ^{54}Fe, ^{52}Fe, decaying to ^{52}Cr, and ^{55}Co, decaying to ^{55}Mn. In general, all odd-*Z* elements of the Fe group Sc, V, and Co are underproduced;

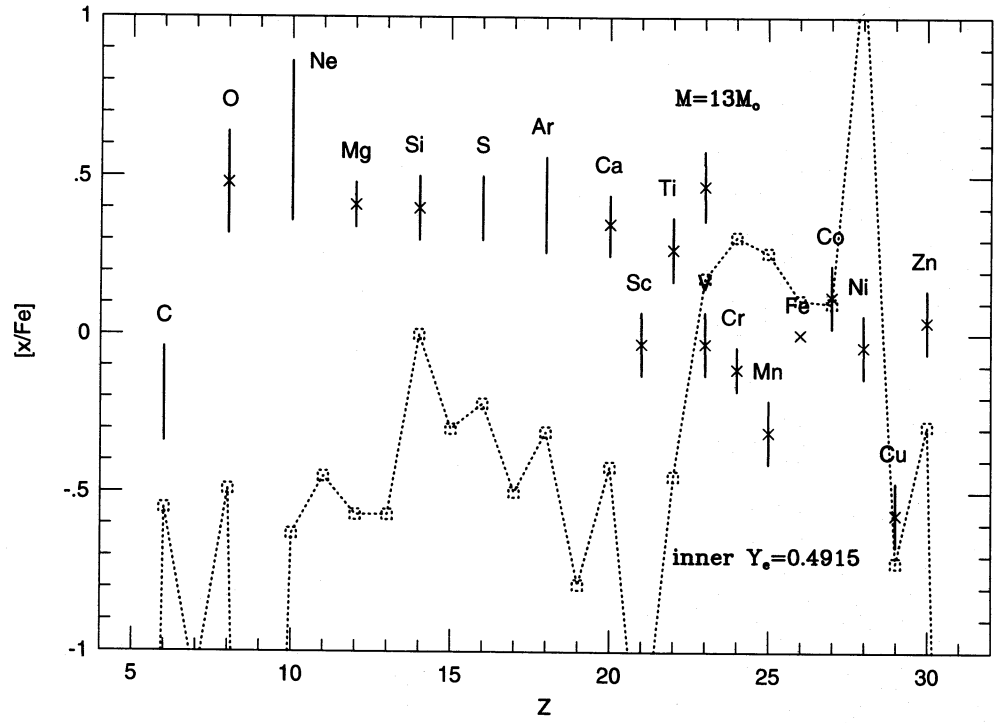

FIG. 5g

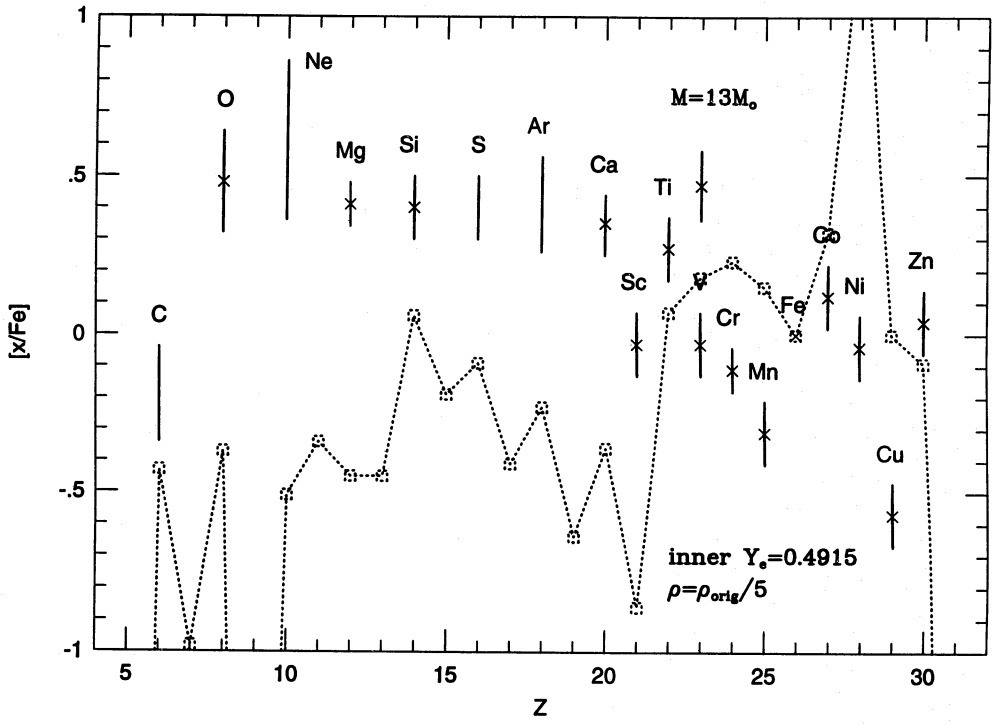

FIG. 5h

the exception is Mn, which was mentioned above. We will see later that this is a feature which is strongly dependent on Y_e.

The behavior of a 20 $M_\odot$ star is shown in Figure 5*b* with a Y_e corresponding to the dashed curve in Figure 2*c*. We see in comparison to Figure 5*a* a reduction in the C-Mg yields, as expected with decreasing progenitor mass. But we also recognize a decrease of explosive O-burning products from S to Ca. This can be explained by a larger amount of ejected ^{56}Ni (^{56}Fe). Thus, only slightly varying S-Ca ejecta can lead to a stronger variation in [x/Fe] if the Fe ejecta actually increase. There seems to be sufficient material in the alpha-rich freezeout to account for ^{48}Ti. The small reduction of Y_e in the inner ejecta to 0.4985 leads to an increase in the odd-Z nuclei of the Fe group, which almost fit the low-metallicity observations. A further decrease in Y_e by adding only 0.01 $M_\odot$ of $Y_e = 0.497$ matter leads to a continued increase of odd-Z elements, like V, Mn, Co, and Cu. However, this is accompanied by a strong increase of the Ni abundance. The reason is that in an alpha-rich freezeout the

neutron-rich ^{54}Fe (in comparison to the dominant ^{52}Fe decaying to ^{52}Cr) is processed to ^{58}Ni and ^{62}Zn (decaying to stable ^{62}Ni). The even further processed ^{68}Ge decays to ^{66}Zn and causes the enhanced population of Zn. The 57/56 (Ni decaying to Fe) ratios observed in SN 1987A suggest the results from Figure 5*b* with only slightly decreased Y_e and slightly enhanced Ni.

Figures 5*d* and 5*e* feature the 15 $M_\odot$ star, both with the $Y_e = 0.4988$ corresponding to the dashed line in Figure 2*b*. Figure 5*d* is identical to the constant entropy case of Figure 1*c*; Figure 5*e* allows a variation of entropies, resulting on average in a higher entropy. This is recognized by the enhanced Ti abundance. In both cases there is a decreasing amount of incomplete Si-burning material involved, which explains the low Cr and Mn abundances. The further decrease of C-Mg is expected from the stellar models. The O burning shows a small decrease as well, owing to the further enhancement of Ni/Fe ejecta as discussed above.

Figures 5*f*–5*h* display the properties of the 13 $M_\odot$ models. Figure 5*f* for $Y_e = 0.4989$ resembles Figures 5*d* and 5*e* in its Fe group composition for the reasons mentioned before. As expected, C-Mg decreases further, and the O-burning products S-Ca are similar to Figure 5*d*. Figure 5*g* shows the tremendous change in the Fe group composition if the Y_e is reduced to 0.4913. It is obvious that such a composition with a huge Ni overabundance cannot play a major role in SN II ejecta, especially as weighting these results with an initial mass function would favor the low-mass end of SNe II clearly over more massive stars. The test whether a reduction in ρ by a factor of 5, i.e., an increase of the entropy by the same amount, dominated by the radiation entropy $S_\gamma = (4/3)aT^3/\rho$, can improve these abundance features results in a failure, as Figure 5*h* indicates. The situation actually worsens. This was performed to test the effect of a very alpha-rich freezeout on the neutron-rich (low Y_e) composition of the inner mass zones.

It is interesting to note at this point that already early attempts to fit solar abundances with a superposition of parameterized explosive nucleosynthesis products (as referenced, e.g., in Trimble 1975) avoided the Y_e range discussed here. Optimal sets for explosive Si burning contained a mixture of products with $Y_e = 0.499$ and 0.46, respectively. In the first case, ^{56}Ni dominates the Fe group completely (being a $Z = A/2$ nucleus), while the second case is dominated by ^{56}Fe (with $Z/A = 0.464$). We now know that this second condition is realized by SNe Ia (see, e.g., Nomoto, Thielemann, & Yokoi 1984; Thielemann, Nomoto, & Yokoi 1986). Any sizable admixture of matter with intermediate Y_e values is problematic, and delayed detonation models for SNe Ia try to make these mass zones as small as possible (Woosley 1990; Khokhlov 1991a, b; Woosley & Weaver 1994). There is also no room for such matter in SNe II ejecta, except maybe very minor amounts originating from the high-entropy bubble.

It has now to be tested whether an integration over an initial mass function with an extended number of progenitor mass grid points for SNe II can fully reproduce the observational constraints from low-metallicity stars. This will be performed in a forthcoming paper (Hashimoto et al. 1995). Such an extended grid is necessary as we neglected contributions by SNe II in the mass range 8–13 $M_\odot$ and beyond 25 $M_\odot$. The 8–10 $M_\odot$ stars will undergo collapse to neutron star densities initiated by *e*-capture in a strongly degenerate core (Miyaji et al. 1980; Nomoto 1984, 1987; Hashimoto et al. 1993a). In addition, 10–13 $M_\odot$ stars are strongly affected by core degeneracy and have a very steep density gradient at the edge of the Fe core (Nomoto & Hashimoto 1988). In both cases, minor amounts of explosive nucleosynthesis ejecta are expected (see, e.g., the Crab Nebula), although it is not completely clear whether these are negligible. The C/O ratio in the hydrostatic C cores will be larger than for more massive stars and with the strong statistical weight of the lower mass stars (IMF), the [C/Fe] will increase and the [O/Fe] ratio will decrease. We will have to see whether, when doing so, one obtains a picture which is consistent with observations.

Ni(Fe) ejecta being a constant or increasing as a function of the progenitor mass might have to be considered as well. This would increase the ratios of [S-Ca/Fe] for the lower mass SNe II, which could be required in order to meet the observed abundance ratios. Observational evidence for the correct behavior can only come from [x/Fe] ratios for stars with [Fe/H] $\lesssim -2.5$, where (in time) the lower mass core-collapse supernovae could not have exploded yet and only more and more massive stars are contributing with decreasing [Fe/H]. At [Fe/H] ≈ -4, one would expect [x/Fe] ratios which are only affected by stars with masses $M > 30$ $M_\odot$ and dominated by the least massive one of those, because of the steep slope of the IMF. Our tables do not yet include such massive stars, so we take the yields of the 25 $M_\odot$ star as a close estimate. Here we find [Mg/Fe] ≈ 1.11 and [Ca/Fe] ≈ 0.37 for the masses of ejected Fe as listed in Table 3. This seems to coincide with the observations by Molaro & Bonifacio (1990) and would be a very encouraging result. It should also be mentioned that Sneden et al. (1994) found another very low-metallicity star with [Fe/H] $= -3.1$, which shows a similar behavior for Ca but which has [Mg/Fe] ≈ 0.4 and very high [Si/Fe] ≈ 1. It is possible that at these low metallicities one picks up witnesses of individual supernova explosions in which, dependent on the progenitor mass, hydrostatic Ne burning stopped at Mg or went all the way to Si. It would be important to find [O/Fe] for both stars. We have also to be aware of the fact that the mass of ejected Fe for $M > 30$ $M_\odot$ is very uncertain. A comparison awaits a reevaluation of [Fe/H] and a complete galactical evolution calculation with these new yields. A complete survey over more such low-metallicity objects (Beers, Preston, & Shectman 1992) can give the final evidence for the correct choice of the neutron star mass cut.

5. CONCLUSIONS

The present paper gives predictions for the detailed isotopic composition of core-collapse supernovae, originating from 13, 15, 20, and 25 $M_\odot$ stars. For assessing the reliability of these predictions, one has to study the different types of uncertainties entering the calculations and how they might be tested.

In the outer zones of ejected material, the composition after an SN II is only a function of the stellar structure [$\rho(r)$, $T(r)$, $Y_i(r)$] alone and contains unprocessed layers, which only reflect the composition resulting from stellar evolution. ^{12}C and ^{16}O are predominantly originating from such mass zones. The comparison with abundances from specific supernova observations (e.g., SN 1987A and 1993J, a 20 $M_\odot$ and an ≈ 15 $M_\odot$ star during their main sequence) seems to give excellent agreement with observed oxygen masses (1.48 vs. 1.3–1.5 $M_\odot$ and 0.42 vs. ≈ 0.4 $M_\odot$). This

indicates that at least the 15 and 20 $M_\odot$ models seem to mimic reality.

The composition of deeper layers is a function of stellar structure and explosive burning. SN 1987A showed reasonable agreement in addition to C and O with Si, Cl, and Ar from our 20 $M_\odot$ model. Supernova remnants like G292.0+1.8 and N132D make it harder to find a connection with the progenitor mass, but it is possible to compare the observational results from optical, UV, and X-ray observations with the whole set of models. For the relative abundance ratios, one finds a very good agreement with an ≈ 20 $M_\odot$ star for N132D and an ≈ 25 $M_\odot$ star for G292.0+1.8. Thus, we have among the listed supernovae and supernova remnants a good abundance agreement with our models for 15, 20, and 25 $M_\odot$.

The amount of detected ^{16}O and ^{12}C and of products from carbon and explosive oxygen burning make it possible to constrain our knowledge of the *effective* $^{12}C(\alpha, \gamma)^{16}O$ rate in He burning. While we cannot make clear statements about the nuclear rate alone, it seems that the combined effect of the nuclear $^{12}C(\alpha, \gamma)^{16}O$ rate and the convection treatment during stellar evolution is predicted well by our choice, the rate of Caughlan et al. (1985, about a factor of 2.3 larger than that of Caughlan & Fowler 1988) and the Schwarzschild criterion of convection without overshooting during the evolution of constant-mass He cores.

The ^{57}Ni/^{56}Ni ratio observed in SN 1987A via γ-rays from ^{56,57}Co decay and spectral features changing during the decay determine the Y_e in the innermost ejected zones. When relying on the 20 $M_\odot$ stellar model, this requires a delay/accretion period of 0.3–0.5 s. Such short delay times are possible for neutrino transport from the proto–neutron star core via convective overturn and seem not possible with neutrino transport via diffusion alone. This agrees with the finding of multidimensional self-consistent hydro calculations for massive SNe II.

For other stellar models, such observations are not yet available, but we can compare the ejected composition to abundances in low-metallicity stars, which reflect the average Type II supernovae composition integrated over an initial mass function of progenitor stars. The mass grid presented here is not fine and extended enough yet to perform such an integration. This will be the topic of a forthcoming paper. We can, however, make some judgment already. The 13 $M_\odot$ star would have the largest statistical weight in our sample, and therefore strong deviations for the Fe group composition from low-metallicity stars should not be allowed. Again, when relying on our model, this would imply delay times beyond 1 s, in order not to eject low-Y_e material, and an explosion more driven by neutrino diffuson. Earlier hydro calculations have shown a strong sensitivity to details such as the nuclear equation of state, determining convective (in)stability. Therefore, such a behavior seems feasible but has to be tested with self-consistent calculations.

The calculations made use of mass cuts between the central neutron star and the ejecta, requiring ejected ^{56}Ni masses as deduced from supernova light-curve observations. Thus, the mass cuts reported here are located at the innermost fully ejected layers and do not contain material which will eventually fall back. This, together with a choice of delay times, leads to predictions of neutron star masses produced in these explosions. The masses given in Table 5 show a significant spread. Two effects can reduce this: (i) decreasing delay times as a function of stellar mass, as discussed above, and (ii) a different set of ^{56}Ni ejecta than used in our Table 3. These were deduced from supernova light-curve observations, but a flatter behavior of the order of 0.07–0.1 $M_\odot$ for all progenitors up to 20 $M_\odot$ seems also permissible. The combination of both effects can increase the predicted M_g for the 13 $M_\odot$ progenitor from 1.16 $M_\odot$ (in case of 0 s delay and 0.15 $M_\odot$ of ^{56}Ni ejecta) to 1.33 $M_\odot$ (for 2 s delay and 0.1 $M_\odot$ of ^{56}Ni ejecta). We have to admit that the conclusions, presented in these last two paragraphs, are somewhat speculative, given the uncertainties involved in the stellar models. They might, nevertheless, be inspiring for future research.

One of the additional constraints which these calculations have to address in the future is the application of a complete progenitor set to chemical evolution calculations (see, e.g., Timmes et al. 1995; Tsujimoto et al. 1995). This will provide an additional test for the stellar models, which have to yield the correct abundance ratios observed in low-metallicity stars, and it also tests the choice of the mass cut by requiring the correct total amount of Type II supernovae Fe production.

We want to thank our collaborators T. Shigeyama and T. Tsujimoto, who contributed to material presented here, and R. Azuma, C. Fransson, R. Gallino, P. Höflich, J. Houck, J. Hughes, K. Langanke, N. Langer, and B. Schmidt for helpful discussions and providing results before publication. This research was supported in part by NSF grant AST 89-13799, the Grants-in-Aid for Scientific Research (05242102, 06233101) and COE research (07E2002) of the Ministry of Education, Science, and Culture in Japan, and the Swiss National Fonds. F. K. T. thanks the Japan Society for the Promotion of Science for supporting an extended stay at the University of Tokyo. The computations were performed at the National Center for Supercomputing Applications at the University of Illinois (AST 890009N).

REFERENCES

Anders, E., & Grevesse, N. 1989, Geochim. Cosmochim. Acta, 53, 197
Arnett, W. D., Bahcall, J. N., Kirshner, R. P., & Woosley, S. E. 1989, ARA&A, 27, 629
Arnett, W. D., & Fu, A. 1989, ApJ, 340, 396
Aufderheide, M., Baron, E., & Thielemann, F.-K. 1991, ApJ, 370, 630
Azuma, R., et al. 1994, Phys. Rev., C50, 1194
Bao, Z. Y., & Käppeler, F. 1987, At. Data Nucl. Data Tables, 36, 411
Barker, F. C., & Kajino, T. 1991, Australian J. Phys., 44, 369
Baron, E., & Cooperstein, J. 1990, in Supernovae, ed. S. E. Woosley (New York: Springer), 342
Baron, E., Hauschildt, P. H., & Young, T. R. 1995, Phys. Rep., 256, 23
Baym, G. 1991, in Neutron Stars, Theory and Observations, ed. J. Ventura & D. Pines (Dordrecht: Kluwer), 37
Beer, H., Voss, F., & Winters, R. R. 1992, ApJS, 80. 403
Beers, T., Preston, G. W., & Schectman, S. A. 1992, AJ, 103, 1987
Bethe, H. A. 1990, Rev. Mod. Phys., 62, 801
Bionta, R. M., et al. 1987, Phys. Rev. Lett., 58, 1494
Blair, W. P., Raymond, J. C., & Long, K. S. 1994, ApJ, 423, 334
Bouchet, P., Danziger, I. J., & Lucy, L. 1991, in SN 1987A and Other Supernovae, ed. I. J. Danziger (Garching: ESO), 217
Brown, G., & Bethe, H. A. 1994, ApJ, 423, 659
Bruenn, S. W. 1989a, ApJ, 340, 955
———. 1989b, ApJ, 341, 385
Bruenn, S. W., & Haxton, W. C. 1991, ApJ, 376, 678
Buchmann, L., et al. 1993, Phys. Rev. Lett., 70, 726
Burrows, A. 1990, Annu. Rev. Nucl. Part. Sci., 40, 181
Burrows, A., & Goshy, J. 1993, ApJ, 416, L75
Burrows, A., Hayes, J., & Fryxell, B. 1995, ApJ, 450, 830

Caughlan, G. R., & Fowler, W. A. 1988, At. Data Nucl. Data Tables, 40, 283
Caughlan, G. R., Fowler, W. A., Harris, M. J., & Zimmerman, G. E. 1985, At. Data Nucl. Data Tables, 32, 197
Chen, J., Dobaczewski, J., Kratz, K.-L., Langanke, K., Pfeiffer, B., Thielemann, F.-K., & Vogel, P. 1995, Phys. Lett. B, 355, 37
Chugai, N. N. 1994, ApJ, 428, L17
Clayton, D. D., Leising, M. D., The, L.-S., Johnson, W. N., & Kurfess, J. D. 1992, ApJ, 399, L14
Clocchiatti, A., Wheeler, J. C., Barker, E. S., Filippenko, A. V., Matheson, T., & Liebert, J. W. 1995, ApJ, 446, 167
Cooperstein, J., & Baron, E. 1989, in Supernovae, ed. A. Petschek (New York: Springer), 213
Cowan, J. J., Thielemann, F.-K., & Truran, J. W. 1991, Phys. Rep., 208, 267
d'Antona, F., & Mazzitelli, I. 1991, in IAU Symp. 145, Evolution of Stars: The Photospheric Abundance Connection, ed. G. Michaud & A. Tutukov (Dordrecht: Kluwer), 399
Danziger, I. J., Bouchet, P., Gouiffes, C., & Lucy, L. 1990, in Supernovae, ed. S. E. Woosley (New York: Springer), 69
Elias, J. H., Depoy, D. L., Gregory, B., & Suntzeff, N. B. 1991, in SN 1987A and Other Supernovae, ed. I. J. Danziger (Garching: ESO), 293
Filippone, B. W., Humblet, J., & Langanke, K. 1989, Phys. Rev., C40, 515
Fransson, C., Houck, J., & Kozma, C. 1995, in IAU Coll. 145, Supernovae and SN Remnants, ed. R. McCray (Cambridge: Cambridge Univ. Press), in press
Fransson, C., & Kozma, C. 1993, ApJ, 408, L25
Freedman, W., et al. 1994, ApJ, 427, 628
Fuller, G. M., Fowler, W. A., & Newman, M. 1980, ApJS, 42, 447
———. 1982, ApJS, 48, 279
———. 1985, ApJ, 293, 1
Gehren, T. 1988, Rev. Mod. Astron., 1, 52
Glendenning, N. K. 1991, Nucl. Phys., B24B, 110
Gratton, R. G., & Sneden, C. 1991, A&A, 241, 501
Hartmann, K., & Gehren, T. 1988, A&A, 199, 269
Hashimoto, M., Iwamoto, K., & Nomoto, K. 1993a, ApJ, 414, L105
Hashimoto, M., Nomoto, K., & Shigeyama, T. 1989, A&A, 210, L5
Hashimoto, M., Nomoto, K., Tsujimoto, T., & Thielemann, F.-K. 1993b, in Nuclei in the Cosmos II, ed. F. Käppeler (Bristol: IOP), 587
———. 1995, in preparation
Herant, M., Benz, W., Hix, W. R., Fryer, C. L., & Colgate, S. A. 1994, ApJ, 435, 339
Hirata, K., et al. 1987, Phys. Rev. Lett., 58, 1490
Houck, J. C., & Fransson, C. 1996, ApJ, 456, 811
Hughes, J. P., & Singh, K. P. 1994, ApJ, 422, 126
Humblet, J. Filippone, B. W., & Koonin, S. E. 1991, Phys. Rev., C44, 2530
Iwamoto, K., Nomoto, K., Höflich, P., Yamaoka, H., Kumagai, S., & Shigeyama, T. 1994, ApJ, 437, L115
Janka, H.-T. 1993, in Frontier Objects in Astrophysics and Particle Physics, ed. F. Giovannelli & G. Mannochi (Bologna: SIF), 345
Janka, H.-T., & Müller, E. 1995, ApJ, 448, L209
Jeffery, D. J., Branch, D., Filippenko, A. V., & Nomoto, K. 1991, ApJ, 448, L109
Khokhlov, A. M. 1991a, A&A, 245, 114
———. 1991b, A&A, 245, L25
Kratz, K.-L., Bitouzet, J.-P., Thielemann, F.-K., Möller, P., & Pfeiffer, B. 1993, ApJ, 402, 216
Kremer, M. U., et al. 1988, Phys. Rev. Lett., 60, 1475
Kumugai, S., Nomoto, K., Shigeyama, T., Hashimoto, M., & Itoh, M. 1993, A&A, 273, 153
Kumugai, S., Shigeyama, T., Hashimoto, M., & Nomoto, K. 1991, A&A, 243, L13
Kurfess, J. D., et al. 1992, ApJ, 399, L137
Lambert, D. L. 1989, in AIP Conf. Proc. 183, Cosmic Abundances of Matter, ed. C. J. Waddington (New York: AIP), 168
Langer, N., & Henkel, C. 1995, in Nuclei in the Cosmos III, ed. M. Busso, R. Gallino, & C. M. Raiteri (New York: AIP), 413
Lattimer, J. M., & Yahil, A. 1989, ApJ, 340, 426
Li, H., & McCray, R. 1992, ApJ, 387, 309
Magain, P. 1989, A&A, 209, 211
Malaney, R. A., & Fowler, W. A. 1988, ApJ, 333, 14
———. 1989, ApJ, 345, L5
Mathews, G. J., Bazan, G., & Cowan, J. J. 1992, ApJ, 391, 719
Matteucci, F. 1987, in ESO Conf. Proc. 27, Stellar Evolution and Dynamics of the Outer Halo of the Galaxy, ed. M. Azzopardi & F. Matteucci (Garching: ESO), 609
Matteucci, F., & Francois, P. 1989, MNRAS, 239, 885
Matteucci, F., Raiteri, C. M., Busso, M., Gallino, R., & Gratton, R. 1993, A&A, 272, 421
Mayle, R. W., & Wilson, J. R. 1988, ApJ, 334, 909
———. 1990, in Supernovae, ed. S. E. Woosley (New York: Springer-Verlag), 333
McCray, R. 1993, ARA&A, 31, 175
Meyer, B. S., Mathews, G. J., Howard, W. M., Woosley, S. E., & Hoffman, R. D. 1992, ApJ, 399, 656
Miyaki, K., Nomoto, K., Yokoi, K., & Sugimoto, D. 1980, PASJ, 32, 303
Mohr, P., et al. 1995, in Nuclei in the Cosmos III, ed. M. Busso, R. Gallino, & C. M. Raiteri (New York: AIP), 243
Molaro, P., & Bonifacio, P. 1990, A&A, 236, L5
Myra, E. S. 1988, Phys. Rep., 163, 127
Myra, E. S., & Bludman, S. 1989, ApJ, 340, 384
Nagase, F. 1989, PASJ, 41, 1
Nissen, P. E., Gustafsson, B., Edvardsson, B., & Gilmore, G. 1994, A&A, 285, 440
Nomoto, K. 1984, ApJ, 277, 791
———. 1987, ApJ, 322, 206
Nomoto, K., Filippenko, A. V., & Shigeyama, T. 1990, A&A, 240, L1
Nomoto, K., & Hashimoto, M. 1988, Phys. Rep., 163, 13
Nomoto, K., Iwamoto, K., & Suzuki, T. 1995, Phys. Rep., 256, 173
Nomoto, K., Suzuki, T., Shigeyama, T., Kumigai, S., Yamaoka, H., & Saio, H. 1993, Nature, 364, 507
Nomoto, K., Thielemann, F.-K., & Yokoi, K. 1984, ApJ, 286, 644
Nomoto, K., Yamaoka, H., Pols, O. R., van den Heuvel, E. P. J., Iwamoto, K., Kumugai, S., & Shigeyama, T. 1994, Nature, 371, 227
Page, D., & Baron, E. 1990, ApJ, 354, L17
Pagel, B. E. J. 1991, Phys. Scr., T36, 7
Panagia, N. 1987, in High Energy Phenomena Around Collapsed Stars, ed. F. Pacini (Dordrecht: Reidel), 33
Peimbert, M. 1992 in Elements and the Cosmos, ed. M. G. Edmunds & R. J. Terlevich (Cambridge: Cambridge Univ. Press), 196
Quillet, J. M. C., et al. 1992, Phys. Rev. Lett., 69, 1896
Rauscher, T., Applegate, J. H., Cowan, J., Thielemann, F.-K., & Wiescher, M. 1994, ApJ, 429, 499
Redder, A., et al. 1987, Nucl. Phys., A462, 385
Schmidt, B. 1995, private communication
Shigeyama, T., Nomoto, K., & Hashimoto, M. 1988, A&A, 196, 141
Shigeyama, T., Nomoto, K., Tsujimoto, T., & Hashimoto, M. 1990, ApJ, 361, L23
Shigeyama, T., Suzuki, T., Kumugai, S., Nomoto, K., Saio, H., & Yamaoka, H. 1994, ApJ, 420, 341
Sneden, C., Preston, G. W., McWilliam, A., & Searle, L. 1994, ApJ, 431, L27
Spyromilio, J., & Pinto, P. A. 1991, in SN 1987A and Other Supernovae, ed. I. J. Danziger & K. Kjär (Garching: ESO/EIPC), 423
Takahashi, K., Witti, J., & Janka, H.-T. 1994, A&A, 286, 857
Thielemann, F.-K., & Arnett, W. D. 1985, ApJ, 295, 604
Thielemann, F.-K., Arnoud, M., & Truran, J. W. 1987, in Advances in Nuclear Astrophysics, ed. E. Vangioni-Flam et al. (Gif sur Yvette: Editions Frontières), 525
Thielemann, F.-K., Hashimoto, M., & Nomoto, K. 1990, ApJ, 349, 222
Thielemann, F.-K., Kratz, K.-L., Pfeiffer, B., Rauscher, T., van Wormer, L., & Wiescher, M. 1994a, Nucl. Phys. A, A570, 329c
Thielemann, F.-K. Nomoto, K., & Hashimoto, M. 1993, in Origin and Evolution of the Elements, ed. N. Prantzos, E. Vangioni-Flam, & M. Cassé (Cambridge: Cambridge Univ. Press), 297
———. 1994b, in Supernovae, Les Houches, Session LIV, ed. S. Bludman, R. Mochkovitch, & J. Zinn-Justin (Amsterdam: Elsevier), 629
Thielemann, F.-K., Nomoto, K., & Yokoi, K. 1986, A&A, 158, 17
Timmes, F., Woosley, S. E., & Weaver, T. A. 1995, ApJS, 98, 617
Trimble, V. 1975, Rev. Mod. Phys., 47, 877
Tsujimoto, T., Nomoto, K., Yoshii, Y., Hashimoto, M., Yanagida, S., & Thielemann, F.-K. 1995, MNRAS, 277, 945
van Paradijs, J. A. 1991, in Neutron Stars, Theory and Observations, ed. J. Ventura & D. Pines (Dordrecht: Kluwer), 289
van Wormer, L., Wiescher, M., Görres, J., Iliadis, C., & Thielemann, F.-K. 1994, ApJ, 432, 326
Varani, G.-F., Meikle, W. P. S., Spyromilio, J., & Allen, D. A. 1990, MNRAS, 245, 570
Weaver, T. A., & Woosley, S. E. 1980, in Ann. NY Acad. Sci., 366, Texas Conference on Relativistic Astrophysics, ed. J. Ehlers, 335
———. 1993, Phys. Rep., 227, 65
Weber, F., & Glendenning, N. K. 1991, Phys. Lett., B265, 1
Werner, K., Dreizler, S., Heber, U., & Rauch, T. 1995, in Nuclei in the Cosmos III, ed. M. Busso, R. Gallino, & C. M. Raiteri (New York: AIP), 45
Wheeler, J. C., & Harkness, R. P. 1990, Rep. Prog. Phys. 53, 1467
Wheeler, J. C., Sneden, C., & Truran, J. W. 1989, ARA&A, 27, 279
Wiescher, M., Görres, J., Graaf, S., Buchmann, L., & Thielemann, F.-K. 1989, ApJ, 343, 352
Wiescher, M., Görres, J., & Thielemann, F.-K. 1990, ApJ, 363, 340
Wiescher, M., Görres, J., Thielemann, F.-K., & Ritter, H. 1986, A&A, 160, 56
Wiescher, M., Harms, V., Görres, J., Thielemann, F.-K., & Rybarcyk, L. J. 1987, ApJ, 316, 162
Wilson, J. R., & Mayle, R. W. 1988, Phys. Rep., 163, 63
———. 1993, Phys. Rep., 227, 97
Witteborn, F. C., Bregman, J. D., Wooden, D. H., Pinto, P. A., Rank, D. M., Woosley, S. E., & Cohen, M. 1989, ApJ, 338, L9
Witti, J., Janka, H.-T., & Takahashi, K. 1994, A&A, 286, 841
Wooden, D. H., Rank, D. M., Bregman, J. D., Witteborn, E. C., Cohen, M., Pinto, P. A., & Axelrod, T. S. 1993, ApJS, 88, 477
Woosley, S. E. 1988, ApJ, 330, 218
———. 1990, in Supernovae, ed. A. G. Petcheck (Berlin: Springer), 182
Woosley, S. E., Arnett, W. D., & Clayton, D. D. 1973, ApJS, 26, 231
Woosley, S. E., Eastman, R. G., Weaver, T. A., & Pinto, P. P. 1994, ApJ, 429, 300
Woosley, S. E., & Hoffman, R. 1992, ApJ, 395, 202

Woosley, S. E., Mathews, G. J., Wilson, J. R., Hoffman, R. D., & Meyer, B. S. 1994, ApJ, 433, 229
Woosley, S. E., Pinto, P. A., & Weaver, T. A. 1988, Proc. Astron. Soc. Australia, 7, 355
Woosley, S. E., & Weaver, T. A. 1986, ARA&A, 24, 205
———. 1994, in Les Houches, Session LIV, Supernovae, ed. S. R. Bludman, R. Mochkovitch, & J. Zinn-Justin (Amsterdam: Elsevier), 63
Young, T. R., Baron, E., & Branch, D. 1995, ApJ, 449, L51
Zhao, Z., France, R. H., Lai, K. S., Rugari, S. L., Gai, M., & Wilds, E. L. 1993a, Phys. Rev. Lett., 70, 2066
Zhao, Z., et al. 1993b, Phys. Rev., C48, 429
Zhao, G., & Magain, P. 1990, A&A, 238, 242